R. Vescovini, V. Oliveri, D. Pizzi, L. Dozio, P.M. Weaver
A Semi-Analytical Approach for the Analysis of Variable-Stiffness Panels with Curvilinear Stiffeners
International Journal of Solids and Structures, In press - Published online 23/10/2019
doi:10.1016/j.ijsolstr.2019.10.011

A Semi-Analytical Approach for the Analysis of Variable-Stiffness Panels with Curvilinear Stiffeners

Riccardo Vescovini[a,1], Vincenzo Oliveri[b], Davide Pizzi[a], Lorenzo Dozio[a], Paul M. Weaver[b]

[a] *Dipartimento di Scienze e Tecnologie Aerospaziali, Politecnico di Milano*
Via La Masa 34
20156 Milano, Italy
[b] *School of Engineering and Bernal Institute, University of Limerick, Ireland*

⋆Declarations of interests: none.

⋆⋆Acknowledgments: Vincenzo Oliveri and Paul M. Weaver would like to thank Science Foundation Ireland for funding the Spatially and Temporally Variable Composite Structures (Varicomp) grant no. (15/RP/2773) under its Research Professor program.

Email address: riccardo.vescovini@polimi.it (Riccardo Vescovini)

Preprint submitted to Elsevier

Abstract

A semi-analytical method is developed for the analysis of composite stiffened panels, where stiffness variability is achieved through a combination of fiber steering and curvilinear stringers. The approach relies upon a 2D plate model for the skin and a 1D beam description for the stiffeners, according to first-order shear deformation theory. The approach is developed in the framework of a displacement-based formulation, where Legendre polynomials are used for approximating the displacement field, and the Ritz method is used for the solution strategy. The resulting tool is characterized by its excellent computational efficiency, and allows problems in free-vibrations, buckling and thermal buckling to be solved with reduced effort. The quality of the results is assessed by an extensive set of comparison against results from the literature, demonstrating the potential of the tool as a means for performing preliminary parametric studies for these variable-stiffness, variable-geometry structures.

Keywords: Variable-stiffness; curvilinear stiffeners; Ritz method; buckling; free-vibrations.

1. Introduction

New manufacturing techniques, such as automated fiber placement (AFP), automated tape laying (ATL) and addictive manufacturing, offer the chance of exploring novel structural configurations and concepts, that in the past were hardly realizable, with the benefits of improved efficiency. This is of particular interest for primary load-carrying structures of aerospace vehicles, for which structural efficiency is among main concerns. In this context, structural panels, such as those employed in wings and fuselages, are classically realized in metallic or straight-fiber composite materials, with architecture based on orthogonal stiffening elements, i.e. stringers and frames or ribs. Taking advantage of technologies now available, major gains could be achieved through a variable-stiffness (VS) design philosophy, where a variable-stiffness skin – obtained by changing the fiber orientation as function of the planar position – is combined with stiffeners running along arbitrarily curvilinear paths. Indeed, the possibility of arranging non-straight stiffeners can be seen as an alternative way for designing the load paths through localized stiffness distribution. In other words, curvilinear stiffeners can be interpreted as a special case of variable-stiffness panels, where stiffness distribution is achieved by means of Dirac delta functions.
The advantages offered by VS laminates are well-known, and have been extensively studied with respect to their behavior in terms of mechanical buckling [1–10], thermal buckling [11–13], fundamental frequencies [14–16] and failure loads [5, 17]. One side-effect of variable-stiffness configurations is the exponentially growing number of degrees of freedom, which requires special consideration. Therefore, efficient tools are of paramount importance to support the design phase, even more than in the case of classical straight-fiber configurations. With this aim in mind, Ritz-based approaches

were proposed as a valuable mean for achieving accurate results with a relatively few degrees of freedom. Examples can be found in Refs. [6, 7], where buckling and post-buckling analyses are performed in the framework of a mixed formulation along with thin-plane theory. Displacement-based formulations are developed referring to first-order shear deformation theory (FSDT) in Refs. [13, 18] and high-order theories in Ref. [19]. An example of a fast design optimization process of VS panels based on a Ritz-like approach can be found in Ref. [20].

Regarding unconventional stiffening arrangements, an early study due to Gürdal and Grall [21] discusses the modeling of geodesically stiffened panels, an extension of which is given by curvilinear stiffeners, presented in pioneering works due to Kapania and co-workers [22, 23]. Successive studies indicated that reduction of static stresses, improvement of buckling load [24] and weight reduction [25] can be achieved, highlighting the importance of gathering understanding through design optimization.

Modeling of curvilinearly stiffened panels represents a challenge owing to inherent geometrical complexity. Special care is needed to realize finite element models, as possible issues due to element distortion and skin-stringer continuity enforcement have to be taken into account. To overcome this issue, finite element procedures were proposed in Refs. [26–28], where stiffeners displacements are expressed as function of those of the skin reference surface using finite element shape functions. In doing so, the generation of the models is made simpler: skin and stiffener elements can be generated independently from one another, and requirements in terms of shared nodes at the skin/stiffener interface need not be fulfilled.

Mesh-free methods are another strategy particularly suited to handle the modeling issues associated with curvilinearly stiffened panels. Tamijani and Kapania developed element-free Galerkin [29, 30] and Ritz-based approaches [31, 32] for analyzing

isotropic panels under various boundary and loading conditions. The methods were applied to free-vibration [29, 31, 32], bending and buckling [30, 32] problems, and proved to be an effective way for performing parametric and sensitivity studies, allowing insight into the potential offered by curvilinear stiffeners to be gained. Recently, the Ritz approach was extended to composite panels to assess the flutter response of curvilinearly stiffened panels [33].

In the last two years, new studies introduced the idea of combining variable-stiffness skins with curvilinear stiffeners, aiming at exploiting the improved design flexibility to achieve better structural response [34–36]. Singh and Kapania [34] employed NASTRAN analyses and Particle Warm Optimization (PSO) optimization to demonstrate that, under certain loading conditions, a 200% increase is possible in terms of buckling load, compared to classical composite configurations with straight stiffeners. Special purpose finite element models were developed to illustrate advantages in terms of free-vibration response [36], with or without pre-stresses, and thermal buckling behavior [35].

As it turns out, previous studies dealing with combined stiffness variability due to VS skin and curvilinear stiffeners are restricted to finite element procedures. However, the availability of a mesh-free strategy – which is the aim of the present effort – is believed to be beneficial for accurate yet fast predictions, thus facilitating the realization of sensitivity and parametric studies, as well as preliminary design optimizations.

This work illustrates a semi-analytical approach based on the Ritz method, where, following Tamijani and Kapania [31, 32], stiffened panels are described as an assembly of plate and beam elements for modeling skin and stringers, respectively. The approach is developed in the framework of a displacement-based formulation, where

the generalized displacement components are expanded by means of orthogonal polynomials. Specifically, Legendre polynomials are used due to their excellent properties in terms of convergence, stability and sparsity of the resulting matrices [6, 37, 38]. Relatively high number of trial functions, which can be necessary for capturing local modes, are easily handled thanks to the efficiency of the implementation. The numerical tool allows linear static problems to be solved, including static, free-vibration, buckling and thermal buckling ones. Flexibility in design is guaranteed by accounting for any boundary conditions and multiple loads, in terms of prescribed forces and displacements. The quality of the results is assessed by comparison against finite element calculations, illustrating the promise of the proposed tool as a valuable mean for performing preliminary parametric studies and assessing the potential benefits of VS panels with curvilinear stringers.

The paper is organized first by illustrating the variational framework, along with kinematic models used for modeling skin and stiffeners. Then, the Ritz method is introduced, and the approximate expressions for the energy contributions are derived, leading to a final set of discrete governing equations to be solved numerically. Starting from the analysis of unstiffened panels, examples of increasing complexity are illustrated up to the case of variable-stiffness panels with straight and curvilinear stringers.

2. Formulation

The semi-analytical approach described herein allows the fast analysis of flat panels stiffened by an arbitrary number of curvilinear stringers, a sketch of which is shown in Figure 1. The total dimensions of the panel along the longitudinal and transverse dimensions are denoted with a and b, respectively, while the thickness is

t. Blade stiffeners are considered, each one characterized by height h^i and width t^i. The panels are made of composite material, the fiber orientation of the plate having the possibility of varying their orientation across the domain. Therefore, variable-stiffness skins can be modeled, where the stiffnesses of the laminated plate are a function of the planar position. On the contrary, blade stiffeners are realized by stacking straight-fiber plies along the direction normal to the stiffener height. Thus, the ply orientation remains constant along the stiffener axis. Furthermore, the stiffener stacking sequence is assumed to be specially orthotropic.

The loading conditions can be in the form of forces per unit length, applied at any of the four edges, according to the conventions of Figure 1. The components along x and y are indicated as $\overline{N}_{xi}$ and $\overline{N}_{yi}$ for a generic edge i, and they are positive when directed along the positive direction of the axes x and y. The index i varies between 1 and 4 accordingly, as reported in the figure, which also defines the edge numbering scheme used for specifying boundary conditions. For an edge at $x = \text{const}$, the tensile/compressive contribution is $\overline{N}_{xi}$, while the shear is $\overline{N}_{yi}$. Note that the forces in the figure are depicted as constant, but any arbitrary distribution can be modeled. Also, it should be noted that they do not represent a self-balanced system of forces, as they are presented according to their positive directions. In addition, the panel can be loaded by prescribing the edge displacements $\overline{u}_i$ and $\overline{v}_i$ for both the plate and the stiffeners according to the conventions of Figure 1 . Pressure loads with arbitrary distribution and intensity denoted with p are also considered. Thermal loads, if any, are modeled in the form of uniform temperature changes, where positive values of ΔT denote heating and negative ones cooling.

Any combination of free, simply-supported and clamped conditions at the four edges can be accounted for. The approach allows for the assessment of the linear static,

free-vibration – with or without pre-stresses – and buckling response in the presence of the aforementioned thermo-mechanical loads. The formulation is developed in the context of a variational framework, where the stiffened panel is modeled as an assembly of a plate element representative of the skin, and beam elements for the stiffeners. Firstly, the variational principle is presented. Then, the kinematics and energy contributions for the plate and the stiffeners are discussed, illustrating the conditions necessary for guaranteeing the compatibility of the displacements at the plate/stiffener interface. Finally, the governing equations are derived by using the Ritz method.

2.1. Variational approach

The formulation is developed by referring to an energy approach, presented here to consider various types of analyses into a unique, compact expression [39]. The relevant functional is denoted as F and can be written as:

$$F = F_{\mathrm{p}} + \sum_{i=1}^{\mathrm{N_s}} F^i \tag{1}$$

As shown, the functional is obtained as the sum of the contributions due to the plate, F_{p}, and those of the $\mathrm{N_s}$ stiffeners, F^i. Note, hereinafter the superscript i is used to denote any quantity referred to the generic i-th stiffener. The two terms entering the functional of Eq. (1) are available as:

$$F_{\mathrm{p}} = U - \beta_1 W - \beta_2 W_{\mathrm{b}} - \beta_3 K \tag{2}$$

and:

$$F^i = U^i - \beta_1 W^i - \beta_2 W^i_{\mathrm{b}} - \beta_3 K^i \tag{3}$$

where β_i are Boolean flags, whose values are chosen according to Table 1, and leading to different interpretations for F: for the linear static case, it is the total potential

energy, Π; for free-vibration analysis, it is the maximum potential energy during the harmonic oscillation; in case of buckling, the functional F is the second variation of the potential energy, $\delta^2\Pi$.

The terms W and W^i of Eqs. (2) and (3) are the negative potentials of external loads and account for mechanical and thermal effects, whilst W_b is the pre-load contribution to $\delta^2\Pi$ in case of buckling analysis.

Irrespective of the type of analysis, the governing equations are available by imposing the stationary condition as:

$$\delta F = 0 \tag{4}$$

and, considering a Ritz approximation, where the N generalized coordinates are denoted as a_i, the set of discrete equations corresponding to Eq. (4) are written as:

$$\frac{\partial F}{\partial a_i}\delta a_i = 0 \qquad \forall \delta a_i \tag{5}$$

2.2. Skin

A two-dimensional plate model is employed for representing the skin of the stiffened panel. A sketch is reported in Figure 2 where dimensions, fiber orientations and conventions for the kinematic variables are provided. A Cartesian reference system xyz is taken over the plate midsurface, with the origin located in the middle of the plate. The x and y axes define the longitudinal and transverse directions, while z runs along the thickness. The dimensions of the plate are a and b, and correspond to the total dimensions of the stiffened panel.

Variable-stiffness configurations are considered by assuming that the fibers are oriented with different angles at given locations of the plate domain. In particular, a grid of arbitrarily distributed $M \times N$ points is considered, where the orientation angles are specified as θ_{mn} over one quarter of the plate, as illustrated in Figure 2(a).

These angles are interpolated by means of Lagrange polynomials, and the function describing the ply orientation over the plate domain is obtained as [6]:

$$\theta(x,y) = \sum_{m=0}^{M-1}\sum_{n=0}^{N-1}\theta_{mn}\prod_{m\neq i}\left(\frac{|x|-x_i}{x_m-x_i}\right)\prod_{n\neq j}\left(\frac{|y|-y_j}{y_n-y_j}\right) \tag{6}$$

In general, the description is non-linear with respect to the x and y coordinates. A linear variation can be retrieved as a special case by considering just two points at the center and the edge of the plate. If so, the corresponding orientations θ_0 and θ_1, along with the rotation Φ of the local reference system, are summarized in the compact notation $[\Phi < \theta_0|\theta_1 >]$.

It is worth mentioning that the representation of Eq. (6) can be inadequate whenever orientation angles are prescribed in several points due to Runge's phenomenon. In the present work all comparisons are discussed against reference results based on the description of Eq. (6), which is then retained for consistency. To a more general extent, alternative representations based on Chebyshev nodes or Legendre interpolating functions should be considered as valuable alternatives to avoid the above mentioned issue.

Kinematics

The kinematic model of the plate is developed on the basis of the First Order Shear Deformation Theory (FSDT), such that the formulation is not restricted to thin plate analysis. In this context, the displacement field is described as:

$$\begin{aligned}\mathbf{u}(x,y,z) &= \mathbf{u}_0(x,y) + z\mathbf{L}\boldsymbol{\varphi}(x,y)\\ &= [\mathbf{I} \quad z\mathbf{L}]\begin{Bmatrix}\mathbf{u}_0\\ \boldsymbol{\varphi}\end{Bmatrix} = [\mathbf{I} \quad z\mathbf{L}]\,\mathbf{d}_0\end{aligned} \tag{7}$$

where:

$$\mathbf{L} = \begin{bmatrix} 1 & 0 & 0 \\ 0 & 1 & 0 \\ 0 & 0 & 0 \end{bmatrix} \tag{8}$$

and the vector $\mathbf{d}_0$ collects the generalized displacement components $\mathbf{u}_0$ and $\boldsymbol{\varphi}$ of the kinematic model, whose components are:

$$\mathbf{u}_0 = \{u_0 \quad v_0 \quad w_0\}^{\mathrm{T}} \qquad \boldsymbol{\varphi} = \{\varphi_x \quad \varphi_y \quad \varphi_z\}^{\mathrm{T}} \tag{9}$$

The positive directions for the generalized displacement parameters are depicted in Figure 2(b). In view of the next steps, it is noted that the rotations φ_i are not positive according to the right-hand rule convention, but they are rotation parameters based on the usual notation of FSDT [40]. The rotation parameter φ_z is associated with zero plate stiffness, but is introduced here with the purpose of enforcing compatibility conditions with the stiffener beam elements.

Consistently with Eq. (7), the vector of in-plane strain components is organized as:

$$\boldsymbol{\epsilon} = \{\epsilon_{xx} \quad \epsilon_{yy} \quad 2\epsilon_{xy}\}^{\mathrm{T}} = \boldsymbol{\xi} + z\mathbf{k} + \boldsymbol{\eta} \tag{10}$$

where $\boldsymbol{\xi}$ and $\mathbf{k}$ are the vectors of membrane strains and curvatures, respectively , defined as $\boldsymbol{\xi} = \{u_{,x} \;\; v_{,y} \;\; u_{,y} + v_{,x}\}^{\mathrm{T}}$ and $\mathbf{k} = \{w_{,xx} \;\; -w_{,yy} \;\; -2w_{,xy}\}^{\mathrm{T}}$; the term $\boldsymbol{\eta} = \{\frac{1}{2}w_{,x}^2 \;\; \frac{1}{2}w_{,y}^2 \;\; w_{,x}w_{,y}\}^{\mathrm{T}}$accounts for the non-linear contributions on the basis of von Kármán assumptions and is retained only for buckling analysis.

In view of successive derivations, it is useful to define a vector collecting the strain parameters as:

$$\mathbf{e} = \left\{\boldsymbol{\xi}^{\mathrm{T}} \quad \mathbf{k}^{\mathrm{T}} \quad \boldsymbol{\gamma}^{\mathrm{T}}\right\}^{\mathrm{T}} \tag{11}$$

where $\boldsymbol{\gamma} = \{\gamma_{yz} \quad \gamma_{xz}\}^{\mathrm{T}} = \{w_{,y} + \varphi_y \quad w_{,x} + \varphi_x\}^{\mathrm{T}}$ are the transverse shear components.

The thermo-elastic constitutive relation is based on the assumption that the only non-zero components of thermal expansion are those associated with the in-plane behavior, and it is given as:

$$\boldsymbol{\sigma}^{(k)} = \overline{\mathbf{Q}}^{(k)}(x,y)\left(\boldsymbol{\epsilon}^{(k)} - \boldsymbol{\epsilon}_{\mathrm{th}}^{(k)}\right) \qquad \boldsymbol{\tau}^{(k)} = \overline{\mathbf{Q}}_{\mathrm{s}}^{(k)}(x,y)\boldsymbol{\gamma} \tag{12}$$

where $\overline{\mathbf{Q}}^{(k)}$ and $\overline{\mathbf{Q}}_{\mathrm{s}}^{(k)}$ are referred to the generic ply k and expressed in the global reference system. Note, the elastic coefficients are functions of the position because the fibers are, in general, non straight; the term $\boldsymbol{\epsilon}^{(k)}$ is the total deformation, accounting for the mechanical and thermal contributions, the latter available as:

$$\boldsymbol{\epsilon}_{\mathrm{th}}^{(k)} = \overline{\boldsymbol{\alpha}}^{(k)}(x,y)\Delta T \tag{13}$$

where $\overline{\boldsymbol{\alpha}}^{(k)}$ is the ply coefficient of thermal expansion, expressed in the laminate reference system. The force resultants are:

$$\begin{aligned}
\mathbf{N} &= \int_t \boldsymbol{\sigma}^{(k)}\,\mathrm{d}z \;= \mathbf{A}(x,y)\boldsymbol{\xi} + \mathbf{B}(x,y)\mathbf{k} - \hat{\mathbf{N}}(x,y)\Delta T \\
\mathbf{M} &= \int_t z\boldsymbol{\sigma}^{(k)}\,\mathrm{d}z \;= \mathbf{B}(x,y)\boldsymbol{\xi} + \mathbf{D}(x,y)\mathbf{k} - \hat{\mathbf{M}}(x,y)\Delta T \\
\mathbf{Q} &= \int_t \boldsymbol{\tau}^{(k)}\,\mathrm{d}z \;= \mathbf{A}^{\mathrm{s}}(x,y)\boldsymbol{\gamma}
\end{aligned} \tag{14}$$

The matrices $\mathbf{A}$, $\mathbf{B}$, $\mathbf{D}$ and $\mathbf{A}^{\mathrm{s}}$ are the usual membrane, coupling, bending and transverse shear stiffness contributions [40], where dependence on the in-plane position is explicitly indicated; the terms $\hat{\mathbf{N}}$ and $\hat{\mathbf{M}}$ are the unit thermal stress resultants, which are available as:

$$\begin{aligned}
\hat{\mathbf{N}}(x,y) &= \int_t \overline{\mathbf{Q}}^{(k)}\overline{\boldsymbol{\alpha}}^{(k)}(x,y)\,\mathrm{d}z \\
\hat{\mathbf{M}}(x,y) &= \int_t z\overline{\mathbf{Q}}^{(k)}\overline{\boldsymbol{\alpha}}^{(k)}(x,y)\,\mathrm{d}z
\end{aligned} \tag{15}$$

The vector collecting the unit thermal resultants is defined as:

$$\hat{\mathbf{R}} = \left\{ \hat{\mathbf{N}}^{\mathrm{T}} \quad \hat{\mathbf{M}}^{\mathrm{T}} \quad \hat{\mathbf{Q}}^{\mathrm{T}} \right\}^{\mathrm{T}} \tag{16}$$

where the third contribution refers to the transverse shear thermal forces, which are identically null as implied by Eq. (12), i.e $\hat{\mathbf{Q}} = \mathbf{0}$.

Energy contributions

Based on the aforementioned kinematic model and the corresponding constitutive relations, the plate strain energy is written as:

$$U = \frac{1}{2} \int_{\mathrm{A}} \begin{Bmatrix} \boldsymbol{\xi} \\ \mathbf{k} \\ \boldsymbol{\gamma} \end{Bmatrix}^{\mathrm{T}} \begin{bmatrix} \mathbf{A} & \mathbf{B} & \mathbf{0} \\ \mathbf{B} & \mathbf{D} & \mathbf{0} \\ \mathbf{0} & \mathbf{0} & \mathbf{A}^{\mathrm{s}} \end{bmatrix} \begin{Bmatrix} \boldsymbol{\xi} \\ \mathbf{k} \\ \boldsymbol{\gamma} \end{Bmatrix} \mathrm{dA} = \frac{1}{2} \int_{\mathrm{A}} \mathbf{e}^{\mathrm{T}} \mathbf{D}_{\mathrm{p}} \mathbf{e} \, \mathrm{dA} \tag{17}$$

where vector $\mathbf{e}$ is defined by Eq. (11), while the matrix $\mathbf{D}_{\mathrm{p}}$ provides a compact description of the plate constitutive behavior. The strain energy can be re-written in terms of the generalized displacement components by recalling Eq. (7) and introducing the differential matrix $\boldsymbol{\mathcal{B}}_{\mathbf{1}}$, whose expression is available in the Appendix, so obtaining:

$$U = \frac{1}{2} \int_{\mathrm{A}} \left(\boldsymbol{\mathcal{B}}_{\mathbf{1}} \mathbf{d}_0 \right)^{\mathrm{T}} \mathbf{D}_{\mathrm{p}} \boldsymbol{\mathcal{B}}_{\mathbf{1}} \mathbf{d}_0 \, \mathrm{dA} \tag{18}$$

The contribution due the external loads W reads:

$$W = \int_{\mathrm{A}} wp \, \mathrm{dA} + \sum_{i=1}^{4} \int_{\partial \mathrm{A_i}} \left(u_0 \overline{N}_{xi} + v_0 \overline{N}_{yi} \right) \mathrm{d}\partial \mathrm{A}_i + \int_{\mathrm{A}} \mathbf{e}^{\mathrm{T}} \hat{\mathbf{R}}(x, y) \, \mathrm{dA} \, \Delta T \tag{19}$$

where the first term refers to the external pressure p, and the second accounts for prescribed forces along the four edges, following the conventions of Figure 1. The last term accounts for temperature variations and use is made of Eqs. (11) and (16)

when introducing the unit thermal resultants.

The fourth contribution of Eq. (2) stems from the linearization of the non-linear terms of the strain-displacement relation according to von Kármán assumptions, and is written as:

$$W_{\mathrm{b}} = \frac{1}{2}\int_{\mathrm{A}} \left[N_{xx}(x,y) w_{0,x}^2 + 2N_{xy}(x,y) w_{0,x} w_{0,y} + N_{yy}(x,y) w_{0,y}^2 \right] \mathrm{dA} \tag{20}$$

It is important to note that, in general, the pre-buckling force resultants N_{ik} are a function of the position (x, y), which are determined by means of an initial pre-buckling analysis.

The last contribution in the functional in Eq. (2) is associated with the kinetic energy, and is relevant in the context of free-vibration problems. Within the present kinematic assumptions and referring to Eq. (7), the kinetic energy is obtained as:

$$K = \frac{1}{2}\int_{\mathrm{A}} \begin{Bmatrix} \mathbf{u}_0 \\ \boldsymbol{\varphi} \end{Bmatrix}^{\mathrm{T}} \int_t \rho_0 \begin{bmatrix} \mathbf{I} & z\mathbf{L} \\ z\mathbf{L} & z^2\mathbf{L} \end{bmatrix} \mathrm{d}z \begin{Bmatrix} \ddot{\mathbf{u}}_0 \\ \ddot{\boldsymbol{\varphi}} \end{Bmatrix} \mathrm{dA} = \frac{1}{2}\int_{\mathrm{A}} \mathbf{d}_0^{\mathrm{T}} \mathbf{m} \ddot{\mathbf{d}}_0 \, \mathrm{dA} \tag{21}$$

where $\mathbf{m}$ is the mass matrix obtained by performing the thickness integral on the right-hand side of Eq. (21).

2.3. Stiffeners

The second structural component of the stiffened panel is given by the stiffeners. The model is restricted here to the case of blade stiffeners, obtained in the form of laminates with constant ply orientations. The geometry is described using Bézier curves, while the kinematic model refers to first order beam theory.

Geometry

The stiffener path is parameterized using a Bézier description. Specifically, the stiffener coordinates $\mathbf{x} = \{x \quad y \quad z\}^{\mathrm{T}}$ are expressed by the vector-valued function

$\mathbf{x} = \mathbf{R}(q)$, defined as:

$$\mathbf{R}(q) = \sum_{i=0}^{n} \binom{n}{i} \mathbf{P}_i (1-q)^{n-i} q^i \qquad \text{with } q \in [0 \quad 1] \tag{22}$$

where $\mathbf{P}_i$ are the coordinates of the control points.

Numerical integration is needed within the present Ritz-based procedure, therefore it is useful to express the curve parameterization as function of a parameter $p \in [-1 \quad 1]$. This is done by operating a change of variable in Eq. (22), where $p = 2q - 1$. According to this transformation, third-order Bézier curves can be represented as:

$$\mathbf{R}(p) = \frac{1}{4}(1-p)^2 \mathbf{P}_0 + \frac{1}{2}\left(1-p^2\right)\mathbf{P}_1 + \frac{1}{4}(1+p)^2 \mathbf{P}_2 \qquad \text{with } p \in [-1 \quad 1] \tag{23}$$

where the three control points are used for expressing the path.

Once the stiffener path is available, the unit tangent vector to the stiffener path can be evaluated as:

$$\mathbf{t} = \mathbf{x}_{,s} = \frac{\mathbf{x}_{,p}}{||\mathbf{x}_{,p}||} \tag{24}$$

where s is the arc-length coordinate. From Eq. (24) it can be observed that, in general, $||\mathbf{x}_{,p}|| \neq 1$, unless a parameterization is available with respect to the arc-length s. In this regard, the relation between the parameter p and the arc-length differentials is:

$$\mathrm{d}s = ||\mathbf{x}_{,p}||\,\mathrm{d}p = J_\mathrm{s}\,\mathrm{d}p \tag{25}$$

with J_s representing the Jacobian of the transformation between p and s. From Eq. (25) any derivative with respect to the arc-length parameter is obtained as:

$$(\cdot)_{,s} = \frac{1}{J_\mathrm{s}}(\cdot)_{,p} \tag{26}$$

The normal vector to the stiffener axis, $\mathbf{n}$, can be obtained by rotating the vector $\mathbf{t}$ of $\pi/2$ radians along the counterclockwise direction. This approach ensures that

the binormal vector $\mathbf{b}$ points toward the plate normal positive direction, avoiding undesirable sudden inversions of the binormal direction along the stiffener path.

Kinematics

A sketch of the stiffener is reported in Figure 3, where the height and width are denoted with h^i and t^i, respectively. A local reference system snb is taken with the origin on the plate midsurface, allowing for simple enforcement of the compatibility conditions between plate and stiffener. The sketch also illustrates also the positive conventions for the parameters of the kinematic model discussed below. Hereinafter the stiffener path is referred to as Γ^i.

Referring to well-known first-order beam theory, the beam displacement components are represented as:

$$\mathbf{u}^i(s,n,b) = \mathbf{u}_0^i(s) + (\mathbf{d}_\times)^{\mathrm{T}}\,\boldsymbol{\theta}^i(s) \tag{27}$$

where $\mathbf{d} = n\mathbf{n} + b\mathbf{b}$, and $\mathbf{d}_\times$ is the second-order tensor such that $\mathbf{d}_\times\mathbf{a} = \mathbf{d}\times\mathbf{a}$ for any arbitrary vector $\mathbf{a}$. The generalized displacement parameters of the kinematic model are collected in the vectors $\mathbf{u}_0^i$ and $\boldsymbol{\theta}^i$, whose components are:

$$\mathbf{u}_0^i = \begin{Bmatrix} u_{0t}^i & u_{0n}^i & u_{0b}^i \end{Bmatrix}^{\mathrm{T}} \qquad \boldsymbol{\theta}^i = \begin{Bmatrix} \theta_t^i & \theta_n^i & \theta_b^i \end{Bmatrix}^{\mathrm{T}} \tag{28}$$

The positive directions are indicated in Figure 3, where the rotations $\boldsymbol{\theta}^i$ are positive according to right hand rule.

Following Refs. [31, 41], the strains are evaluated as:

$$\boldsymbol{\epsilon}^i = \begin{Bmatrix} \epsilon_{tt}^i \\ \gamma_{tn}^i \\ \gamma_{tb}^i \end{Bmatrix} = \begin{Bmatrix} \mathbf{u}_{,s}^i \cdot \mathbf{t} + \eta_{tt}^i \\ \mathbf{u}_{,s}^i \cdot \mathbf{n} + \mathbf{u}_{,n}^i \cdot \mathbf{t} \\ \mathbf{u}_{,s}^i \cdot \mathbf{b} + \mathbf{u}_{,b}^i \cdot \mathbf{t} \end{Bmatrix} \tag{29}$$

or, in compact form, they can be written as:

$$\boldsymbol{\epsilon}^i = \boldsymbol{\xi}^i + (\mathbf{d}_\times)^{\mathrm{T}} \mathbf{k}^i + \boldsymbol{\eta}^i \tag{30}$$

with:

$$\boldsymbol{\xi}^i = \begin{Bmatrix} \xi^i_{tt} \\ 2\xi^i_{tn} \\ 2\xi^i_{tb} \end{Bmatrix} = \begin{Bmatrix} \mathbf{u}^i_{0,s} \cdot \mathbf{t} \\ \mathbf{u}^i_{0,s} \cdot \mathbf{n} - \boldsymbol{\theta}^i \cdot \mathbf{b} \\ \mathbf{u}^i_{0,s} \cdot \mathbf{b} + \boldsymbol{\theta}^i \cdot \mathbf{n} \end{Bmatrix} \qquad \mathbf{k}^i = \begin{Bmatrix} k^i_{tt} \\ k^i_{tn} \\ k^i_{tb} \end{Bmatrix} = \begin{Bmatrix} \boldsymbol{\theta}^i_{,s} \cdot \mathbf{t} \\ \boldsymbol{\theta}^i_{,s} \cdot \mathbf{b} \\ \boldsymbol{\theta}^i_{,s} \cdot \mathbf{n} \end{Bmatrix} \tag{31}$$

where $\boldsymbol{\xi}^i$ is a vector collecting the axial strain and the transverse shear components, while $\mathbf{k}^i$ collects the beam curvatures. The contribution $\boldsymbol{\eta}^i$ accounts for geometrically non-linear terms, and is retained only in the case of buckling analysis.

The kinematic relation of Eq. (27) and the strains of Eq. (30) are expressed as a function of the beam generalized displacement components $\mathbf{u}^i_0$ and $\boldsymbol{\theta}^i$. However, these latter are not free parameters, as they are related to the plate displacement components via compatibility conditions. In particular, the displacement at the intersection between the plate and the beam is subjected to a $\mathcal{C}^0$ continuity requirement, which is expressed as:

$$\begin{cases} \mathbf{u}^i_0 = \mathbf{u}_0|_{\Gamma^i} \\ \boldsymbol{\theta}^i = \boldsymbol{\mathcal{J}}^{\mathrm{T}} \boldsymbol{\varphi}|_{\Gamma^i} \end{cases} \tag{32}$$

where the beam and plate displacement components are expressed in a common reference system, taken as the global one, unless otherwise stated. The matrix $\boldsymbol{\mathcal{J}}$ is defined as:

$$\boldsymbol{\mathcal{J}} = \begin{bmatrix} 0 & 1 & 0 \\ -1 & 0 & 0 \\ 0 & 0 & 1 \end{bmatrix} \tag{33}$$

and accounts for the different conventions employed for describing plate and beam rotations (see Figures 2(b) and 3).

To avoid cumbersome expressions, the notation is simplified by indicating the displacement components along the stiffener path by introducing a tilde, i.e. $\tilde{\mathbf{u}}_0^i \equiv \mathbf{u}_0|_{\Gamma^i}$ and $\tilde{\boldsymbol{\theta}}_0^i \equiv \boldsymbol{\theta}_0|_{\Gamma^i}$.

The enforcement of the compatibility conditions of Eq. (32) allows to express all the stiffener kinematic parameters as function of the plate ones. The relation in terms of generalized displacements is inherently given by Eq. (32), while the one in terms of generalized strain parameters is obtained as:

$$\tilde{\boldsymbol{\xi}}^i = \begin{Bmatrix} \mathbf{t}^{\mathrm{T}}\tilde{\mathbf{u}}_{0,s}^i + \tilde{\eta}_{tt}^i \\ \mathbf{n}^{\mathrm{T}}\tilde{\mathbf{u}}_{0,s}^i - \mathbf{b}^{\mathrm{T}}\boldsymbol{\mathcal{J}}^{\mathrm{T}}\tilde{\boldsymbol{\varphi}}^i \\ \mathbf{b}^{\mathrm{T}}\tilde{\mathbf{u}}_{0,s}^i + \mathbf{n}^{\mathrm{T}}\boldsymbol{\mathcal{J}}^{\mathrm{T}}\tilde{\boldsymbol{\varphi}}^i \end{Bmatrix} \qquad \tilde{\mathbf{k}}^i = \begin{Bmatrix} \mathbf{t}^{\mathrm{T}}\boldsymbol{\mathcal{J}}^{\mathrm{T}}\tilde{\boldsymbol{\varphi}}_{,s}^i \\ \mathbf{n}^{\mathrm{T}}\boldsymbol{\mathcal{J}}^{\mathrm{T}}\tilde{\boldsymbol{\varphi}}_{,s}^i \\ \mathbf{b}^{\mathrm{T}}\boldsymbol{\mathcal{J}}^{\mathrm{T}}\tilde{\boldsymbol{\varphi}}_{,s}^i \end{Bmatrix} \tag{34}$$

where the derivatives with respect to the arc-length parameter are readily available by projecting the gradients onto the tangent direction:

$$\tilde{\mathbf{u}}_{0,s}^i = \nabla\tilde{\mathbf{u}}_0^i \cdot \mathbf{t} \qquad \tilde{\boldsymbol{\varphi}}_{,s}^i = \nabla\tilde{\boldsymbol{\varphi}}^i \cdot \mathbf{t} \tag{35}$$

Energy contributions

The stiffener strain energy is available as:

$$U^i = \frac{1}{2}\int_{\Gamma^i} \begin{Bmatrix} \tilde{\boldsymbol{\xi}}^i \\ \tilde{\mathbf{k}}^i \end{Bmatrix}^{\mathrm{T}} \mathbf{C}^i \begin{Bmatrix} \tilde{\boldsymbol{\xi}}^i \\ \tilde{\mathbf{k}}^i \end{Bmatrix} \mathrm{d}s \tag{36}$$

where the matrix $\mathbf{C}^i$ defines the beam section properties. The derivation of its expression is presented in the Appendix. The strain vectors are given by Eq. (34) and embed the compatibility of the displacements between the plate and the stiffener.

The potential of external loads is written as:

$$W^i = \tilde{\mathbf{u}}_0^i \mathbf{P}|_{s=0}^{s=\Gamma^i} + \int_{\Gamma^i} \begin{Bmatrix} \tilde{\boldsymbol{\xi}}^i \\ \tilde{\mathbf{k}}^i \end{Bmatrix}^{\mathrm{T}} \begin{Bmatrix} \hat{\mathbf{F}}^i \\ \hat{\mathbf{M}}^i \end{Bmatrix} \mathrm{d}s\, \Delta T \tag{37}$$

where $\mathbf{P}$ is a vector collecting the forces applied at the beam ends. Note that in Eq. (37) thermal loads $\hat{\mathbf{F}}^i$ and $\hat{\mathbf{M}}^i$ depend upon the stiffener thermal properties as illustrated in the Appendix.

In case of buckling analysis, the energy contribution is:

$$W_{\mathrm{b}}^i = \frac{1}{2} \int_{\Gamma^i} P^i \tilde{\eta}_{tt}^i \,\mathrm{d}s = \frac{1}{2} \int_{\Gamma^i} P^i \tilde{u}_{0b,s}^{i^2} \,\mathrm{d}s \tag{38}$$

where P_i is the pre-buckling axial force carried by the stiffener.

The kinetic energy reads:

$$K^i = \frac{1}{2} \int_{\Gamma^i} \mathbf{u}^i \rho \ddot{\mathbf{u}}^i \,\mathrm{d}s \tag{39}$$

and, upon substitution of Eq. (27) into Eq. (39):

$$\begin{aligned} K^i &= \frac{1}{2} \int_{\Gamma^i} \begin{Bmatrix} {}_\ell\mathbf{u}_0^i \\ {}_\ell\boldsymbol{\theta}^i \end{Bmatrix}^{\mathrm{T}} \int_{\mathrm{A}} \rho \begin{bmatrix} \mathbf{I} & (\mathbf{d}_\times)^{\mathrm{T}} \\ (\mathbf{d}_\times) & (\mathbf{d}_\times)(\mathbf{d}_\times)^{\mathrm{T}} \end{bmatrix} \mathrm{dA} \begin{Bmatrix} {}_\ell\ddot{\mathbf{u}}_0^i \\ {}_\ell\ddot{\boldsymbol{\theta}}^i \end{Bmatrix} \mathrm{d}s \\ &= \frac{1}{2} \int_{\Gamma^i} \begin{Bmatrix} {}_\ell\mathbf{u}_0^i \\ {}_\ell\boldsymbol{\theta}^i \end{Bmatrix}^{\mathrm{T}} \begin{bmatrix} \mathbf{M}_{\mathrm{uu}} & \mathbf{M}_{\mathrm{u}\theta} \\ \mathbf{M}_{\mathrm{u}\theta}^{\mathrm{T}} & \mathbf{M}_{\theta\theta} \end{bmatrix} \begin{Bmatrix} {}_\ell\ddot{\mathbf{u}}_0^i \\ {}_\ell\ddot{\boldsymbol{\theta}}^i \end{Bmatrix} \mathrm{d}s \end{aligned} \tag{40}$$

The definition of the matrices $\mathbf{M}_{ik}$ is implicit in the expression of Eq. (40); a left subscript ℓ is introduced to highlight that the vectors of generalized displacements are expressed in the stiffener local reference system. Recalling the compatibility conditions of Eq. (32) and introducing the rotation matrix $\mathbf{R}$ from the global to stiffener local system, the local displacements can be expressed as:

$$\begin{aligned} {}_\ell\mathbf{u}_0^i &= \mathbf{R}\mathbf{u}_0^i = \mathbf{R}\mathbf{u}_0|_{\Gamma^i} \\ {}_\ell\boldsymbol{\theta}^i &= \mathbf{R}\boldsymbol{\theta}^i = \mathbf{R}\boldsymbol{\mathcal{J}}^{\mathrm{T}}\boldsymbol{\varphi}|_{\Gamma^i} \end{aligned} \tag{41}$$

Substitution of Eq. (41) into Eq. (40) allows the kinetic energy to be expressed as a function of the plate's generalized displacement components.

2.4. Ritz approximation

The variational formulation derived so far allows the energy functional to be expressed in terms of the six generalized displacement components $\mathbf{u}_0$ and $\boldsymbol{\varphi}$ of the plate. An approximate solution is sought by expanding the unknowns by means of Ritz trial functions. Once the approximation is achieved at functional level, the governing equations are easily retrieved by imposing the stationarity of F through Eq. (5).

The displacements $\mathbf{u}_0$ are expanded as:

$$\mathbf{u}_0 = \begin{bmatrix} \boldsymbol{\phi}_{\mathrm{u}}^{\mathrm{T}}(\xi,\eta) & & \\ & \boldsymbol{\phi}_{\mathrm{v}}^{\mathrm{T}}(\xi,\eta) & \\ & & \boldsymbol{\phi}_{\mathrm{w}}^{\mathrm{T}}(\xi,\eta) \end{bmatrix} \begin{Bmatrix} \mathbf{c}_{\mathrm{u}} \\ \mathbf{c}_{\mathrm{v}} \\ \mathbf{c}_{\mathrm{w}} \end{Bmatrix} + \begin{Bmatrix} \overline{\boldsymbol{\phi}}_{\mathrm{u}}(\xi) + \overline{\boldsymbol{\psi}}_{\mathrm{u}}(\eta) \\ \overline{\boldsymbol{\phi}}_{\mathrm{v}}(\xi) + \overline{\boldsymbol{\psi}}_{\mathrm{v}}(\eta) \\ 0 \end{Bmatrix} = \boldsymbol{\Phi}_{\mathrm{u}}\mathbf{a}_{\mathrm{u}} + \overline{\boldsymbol{\Phi}}_{\mathrm{u}} \tag{42}$$

where $\boldsymbol{\phi}_i$ are column vectors of dimension $R_i \times S_i$ collecting the trial functions for the generalized displacement component $i \in \{u_0, v_0, w_0\}$, expressed in terms of the nondimensional coordinates $(\xi,\eta) \in [-1 \quad 1]$, with $\xi = 2/a$ and $\eta = 2/b$; $\boldsymbol{\Phi}_{\mathrm{u}}$ is the matrix which includes the three sets of trial functions, while $\mathbf{a}_{\mathrm{u}}$ are the corresponding unknown amplitudes; the overline is introduced to denote the trial functions associated with any prescribed displacement along the plate boundaries. Specifically, they are expressed as linear functions of the coordinates ξ and η as:

$$\begin{aligned} \overline{\boldsymbol{\phi}}_{\mathrm{u}} &= \frac{\overline{u}_3 - \overline{u}_1}{2}\xi \qquad & \overline{\boldsymbol{\psi}}_{\mathrm{u}} &= \frac{\overline{u}_4 - \overline{u}_2}{2}\eta \\ \overline{\boldsymbol{\phi}}_{\mathrm{v}} &= \frac{\overline{v}_3 - \overline{v}_1}{2}\xi \qquad & \overline{\boldsymbol{\psi}}_{\mathrm{v}} &= \frac{\overline{v}_4 - \overline{v}_2}{2}\eta \end{aligned} \tag{43}$$

Similarly to the expansion operated in Eq. (42), it is possible to approximate the rotational degrees of freedom as:

$$\boldsymbol{\varphi} = \begin{bmatrix} \boldsymbol{\phi}_{\varphi_x}^{\mathrm{T}}(\xi,\eta) & & \\ & \boldsymbol{\phi}_{\varphi_y}^{\mathrm{T}}(\xi,\eta) & \\ & & \boldsymbol{\phi}_{\varphi_z}^{\mathrm{T}}(\xi,\eta) \end{bmatrix} \begin{Bmatrix} \mathbf{c}_{\varphi_x} \\ \mathbf{c}_{\varphi_y} \\ \mathbf{c}_{\varphi_z} \end{Bmatrix} = \boldsymbol{\Phi}_{\varphi}\mathbf{a}_{\varphi} \tag{44}$$

Grouping Eqs. (42) and (44) into one single expression and recalling Eq. (7), it is possible to express the six unknown displacement components as:

$$\mathbf{d}_0 = \begin{bmatrix} \boldsymbol{\Phi}_{\mathrm{u}} & \mathbf{0} \\ \mathbf{0} & \boldsymbol{\Phi}_{\varphi} \end{bmatrix} \begin{Bmatrix} \mathbf{a}_{\mathrm{u}} \\ \mathbf{a}_{\varphi} \end{Bmatrix} + \begin{Bmatrix} \overline{\boldsymbol{\Phi}}_{\mathrm{u}} \\ \mathbf{0} \end{Bmatrix} = \boldsymbol{\Phi}\mathbf{a} + \overline{\boldsymbol{\Phi}} \tag{45}$$

where $\mathbf{a}$ is the vector of the Ritz unknown amplitudes, whose dimension is equal to the number of degrees of freedom of the problem. Among the various choices for representing the trial functions $\boldsymbol{\phi}_i$ of Eqs. (42) and (44), Legendre polynomials are employed here due to their excellent stability and convergence properties [38, 42]. Specifically, the expansion is performed as:

$$\begin{aligned} \boldsymbol{\phi}_i(\xi,\eta) = b_i(\xi,\eta)\left[P_r(\xi)\otimes P_s(\eta)\right] \quad \text{with} \quad & r = 0,...,R; s = 0,...,S \\ & i \in \left\{u_0, v_0, w_0, \varphi_x, \varphi_y, \varphi_z\right\} \end{aligned} \tag{46}$$

In the expression above, P_k is the k-th Leegndre polynomial, whilst b_i is the boundary function relative to the generalized displacement component i, whose expression reads:

$$b_i(\xi,\eta) = (1-\xi)^{a_1}(1+\xi)^{a_2}(1-\eta)^{a_3}(1+\eta)^{a_4} \tag{47}$$

The coefficients a_i can take zero or unitary values following Table 2, depending on the specified boundary conditions.

2.5. Plate contributions

The Ritz approximation of the energy contributions is derived by introducing the expansion of Eq. (45) into the relevant terms and performing the corresponding surface and line integrals. With this aim in mind, numerical integration is carried out according to a Gauss-Legendre scheme.

The strain energy is available referring to Eq. (18), and can be written as:

$$\begin{aligned} U &= \frac{1}{2}\mathbf{a}^{\mathrm{T}} \int_{-1}^{1}\int_{-1}^{1} \left(\boldsymbol{\mathcal{B}}_1\boldsymbol{\Phi}\right)^{\mathrm{T}} \mathbf{D}\boldsymbol{\mathcal{B}}_1\boldsymbol{\Phi} J \,\mathrm{d}\xi \,\mathrm{d}\eta \,\mathbf{a} + \mathbf{a}^{\mathrm{T}} \int_{-1}^{1}\int_{-1}^{1} \left(\boldsymbol{\mathcal{B}}_1\overline{\boldsymbol{\Phi}}\right)^{\mathrm{T}} \overline{\mathbf{D}}\boldsymbol{\mathcal{B}}_1\overline{\boldsymbol{\Phi}} J \,\mathrm{d}\xi \,\mathrm{d}\eta \,\mathbf{a} \\ &= \frac{1}{2}\mathbf{a}^{\mathrm{T}}\breve{\mathbf{K}}\mathbf{a} - \mathbf{a}^{\mathrm{T}}\breve{\mathbf{F}}_{\mathrm{u}} \end{aligned} \tag{48}$$

where $J = ab/4$ is the Jacobian of the transformation from (x, y) to the nondimensional system (ξ, η).

The first contribution on the right-hand side highlights the plate stiffness matrix $\breve{\mathbf{K}}$; the second one depends upon the presence of prescribed displacements at the boundaries and is in the form of the forcing vector denoted as $\breve{\mathbf{F}}_{\mathrm{u}}$; whenever displacements are not prescribed, the functions $\overline{\boldsymbol{\Phi}}$ are identically null, and the contribution $\breve{\mathbf{F}}_{\mathrm{u}}$ vanishes.

The energy term due to thermo-mechanical loads is determined by referring to Eqs. (19), (42) and (44) and is:

$$\begin{aligned} W = \mathbf{c}_{\mathrm{w}}^{\mathrm{T}} \int_{-1}^{1}\int_{-1}^{1} p\boldsymbol{\Phi}_{\mathrm{w}}^{\mathrm{T}} J \,\mathrm{d}\xi \,\mathrm{d}\eta + \sum_{i=1}^{4} \mathbf{a}_{\mathrm{u}}^{\mathrm{T}} \int_{\partial A} \boldsymbol{\Phi}_{\mathrm{u}}^{\mathrm{T}} \overline{\mathbf{N}}_i \,\mathrm{d}\partial A + \\ + \mathbf{a}^{\mathrm{T}} \int_{-1}^{1}\int_{-1}^{1} \left(\boldsymbol{\mathcal{B}}_1\boldsymbol{\Phi}\right)^{\mathrm{T}} \hat{\mathbf{R}} \,\mathrm{d}\xi \,\mathrm{d}\eta \,\Delta T = \mathbf{c}_{\mathrm{w}}^{\mathrm{T}}\mathbf{F}_{\mathrm{f}}^{\mathrm{w}} + \mathbf{a}_{\mathrm{u}}^{\mathrm{T}}\mathbf{F}_{\mathrm{f}}^{\mathrm{u}} + \mathbf{a}^{\mathrm{T}}\breve{\mathbf{F}}_{\mathrm{th}} = \mathbf{a}^{\mathrm{T}}\breve{\mathbf{F}} \end{aligned} \tag{49}$$

The geometric stiffness of the plate is derived referring to Eq. (20) and is:

$$W_{\mathrm{b}} = \frac{1}{2}\mathbf{a}^{\mathrm{T}} \int_{-1}^{1}\int_{-1}^{1} \left(\boldsymbol{\mathcal{B}}_2\boldsymbol{\Phi}\right)^{\mathrm{T}} \begin{bmatrix} N_{xx}(\xi,\eta) & N_{xy}(\xi,\eta) \\ N_{xy}(\xi,\eta) & N_{yy}(\xi,\eta) \end{bmatrix} \boldsymbol{\mathcal{B}}_2\boldsymbol{\Phi} J \,\mathrm{d}\xi \,\mathrm{d}\eta \,\mathbf{a} = \frac{1}{2}\mathbf{a}^{\mathrm{T}}\breve{\mathbf{K}}_{\mathrm{g}}\mathbf{a} \tag{50}$$

where $\boldsymbol{\mathcal{B}}_2$ is a differential matrix, whose expression is reported in the Appendix, and the pre-buckling force resultants N_{ik} are determined with an initial pre-buckling analysis.

The last plate contribution regards kinetic energy, which is obtained referring to Eqs. (21) and (45), and is:

$$K = \frac{1}{2}\mathbf{a}^{\mathrm{T}} \int_{-1}^{1}\int_{-1}^{1} \mathbf{\Phi}^{\mathrm{T}}\mathbf{m}\mathbf{\Phi} J \,\mathrm{d}\xi \,\mathrm{d}\eta \,\ddot{\mathbf{a}} = \frac{1}{2}\mathbf{a}^{\mathrm{T}}\breve{\mathbf{M}}\ddot{\mathbf{a}} \tag{51}$$

where the term $\breve{\mathbf{M}}$ is the mass matrix of the plate.

2.6. Stiffener contributions

The evaluation of the stiffener contributions is relatively straightforward as far as the energy terms derived in the previous sections are already available as a function of the generalized displacement components of the plate. This consideration implies that the Ritz expansion of Eq. (45) can be directly substituted into the relevant energy terms. However, an intermediate step is necessary to express the generalized strains, i.e. $\tilde{\boldsymbol{\xi}}^i$ and $\tilde{\mathbf{k}}^i$, as a function of the Ritz unknown amplitudes. Referring to Eqs. (32), (35), (42) and (44), the derivatives of the generalized displacement components with respect to the arc-length coordinate s are:

$$\begin{aligned}
\tilde{\mathbf{u}}^i_{0,s} &= \left(\frac{2}{a}\tilde{\mathbf{\Phi}}^i_{\mathrm{u},\xi}t_x + \frac{2}{b}\tilde{\mathbf{\Phi}}^i_{\mathrm{u},\eta}t_y\right)\mathbf{a}_{\mathrm{u}} + \frac{2}{a}\overline{\mathbf{\Phi}}_{\mathrm{u},\xi}t_x + \frac{2}{b}\overline{\mathbf{\Phi}}_{\mathrm{u},\eta}t_y = \mathbf{d}_{\mathrm{u}}\mathbf{a}_{\mathrm{u}} + \overline{\mathbf{d}}_{\mathrm{u}} \\
\tilde{\boldsymbol{\varphi}}^i_{,s} &= \left(\frac{2}{a}\tilde{\mathbf{\Phi}}^i_{\varphi,\xi}t_x + \frac{2}{b}\tilde{\mathbf{\Phi}}^i_{\varphi,\eta}t_y\right)\mathbf{a}_{\varphi} = \mathbf{d}_{\varphi}\mathbf{a}_{\varphi}
\end{aligned} \tag{52}$$

where the terms $\tilde{\mathbf{\Phi}}^i_{\cdot,\cdot}$ indicate the trial function derivatives for the i-th stiffener. Note, according to Eq. (43), the contributions associated with prescribed edge displacements are linear with ξ and η, thus the first derivatives are constant and independent of the position. For this reason, the stiffener index i is unnecessary over the

corresponding terms $\overline{\mathbf{\Phi}}_{.,.}$.

From Eq. (52) and recalling Eq. (34), the stiffener generalized strains can be expressed as:

$$\begin{Bmatrix} \tilde{\boldsymbol{\xi}}^i \\ \tilde{\mathbf{k}}^i \end{Bmatrix} = \begin{bmatrix} \mathbf{t}^{\mathrm{T}}\mathbf{d}_{\mathrm{u}} & \mathbf{0} \\ \mathbf{n}^{\mathrm{T}}\mathbf{d}_{\mathrm{u}} & -\mathbf{b}^{\mathrm{T}}\boldsymbol{\mathcal{I}}^{\mathrm{T}}\tilde{\mathbf{\Phi}}^i_{\varphi} \\ \mathbf{b}^{\mathrm{T}}\mathbf{d}_{\mathrm{u}} & \mathbf{0} \\ \mathbf{0} & \mathbf{t}^{\mathrm{T}}\mathbf{d}_{\varphi} \\ \mathbf{0} & \mathbf{t}^{\mathrm{T}}\mathbf{n}_{\varphi} \\ \mathbf{0} & \mathbf{t}^{\mathrm{T}}\mathbf{b}_{\varphi} \end{bmatrix} \begin{Bmatrix} \mathbf{a}_{\mathrm{u}} \\ \mathbf{a}_{\varphi} \end{Bmatrix} + \begin{Bmatrix} \mathbf{t}^{\mathrm{T}}\overline{\mathbf{d}}_{\mathrm{u}} \\ \mathbf{n}^{\mathrm{T}}\overline{\mathbf{d}}_{\mathrm{u}} \\ \mathbf{b}^{\mathrm{T}}\overline{\mathbf{d}}_{\mathrm{u}} \\ \mathbf{0} \\ \mathbf{0} \\ \mathbf{0} \end{Bmatrix} = \mathbf{H}_1\mathbf{a} + \overline{\mathbf{e}} \tag{53}$$

Introducing Eq. (53) into Eq. (36) leads to the expression for the stiffener strain energy, which is:

$$U^i = \frac{1}{2}\mathbf{a}^{\mathrm{T}} \int_{-1}^{1} \mathbf{H}_1^{\mathrm{T}}\mathbf{C}^i\mathbf{H}_1 J_{\mathrm{s}}\,\mathrm{d}p\,\mathbf{a} + \mathbf{a}^{\mathrm{T}} \int_{-1}^{1} \mathbf{H}_1^{\mathrm{T}}\mathbf{C}^i\overline{\mathbf{e}}J_{\mathrm{s}}\,\mathrm{d}p = \frac{1}{2}\mathbf{a}^{\mathrm{T}}\mathbf{K}^i\mathbf{a} - \mathbf{a}^{\mathrm{T}}\mathbf{F}^i_{\mathrm{u}} \tag{54}$$

with J_{s} defined by Eq. (25), and $\mathbf{K}^i$ and $\mathbf{F}^i_{\mathrm{u}}$ representing the stiffness matrix and the contribution to the vector of external forces due any prescribed displacement, respectively.

External loads are accounted for by Eq. (37), and referring to Eq. (53):

$$W^i = \mathbf{a}^{\mathrm{T}}\mathbf{F}^i_{\mathrm{f}} + \mathbf{a}^{\mathrm{T}} \int_{-1}^{1} \mathbf{H}_1^{\mathrm{T}} \begin{Bmatrix} \hat{\mathbf{F}}^i \\ \hat{\mathbf{M}}^i \end{Bmatrix} J_{\mathrm{s}}\,\mathrm{d}p\,\Delta T = \mathbf{a}^{\mathrm{T}}\mathbf{F}^i \tag{55}$$

which provides the projection of the stiffener thermal loads onto the Ritz trial functions.

The geometric stiffness matrix is available from Eq. (38):

$$W^i_{\mathrm{b}} = \frac{1}{2}\mathbf{a}^{\mathrm{T}} \int_{-1}^{1} \mathbf{H}_2^{\mathrm{T}} P^i \mathbf{H}_2 J_{\mathrm{s}}\,\mathrm{d}p\,\mathbf{a} = \frac{1}{2}\mathbf{a}^{\mathrm{T}}\mathbf{K}^i_{\mathrm{g}}\mathbf{a} \tag{56}$$

where the vector $\mathbf{H}_2$ allows to determine the derivative of the stiffener out-of-plane deflections with respect to the arc-length coordinate s. Analogously to Eq. (52), $\mathbf{H}_2$ is obtained as:

$$\mathbf{H}_2 = \left\{ 0 \quad 0 \quad \mathbf{b}^{\mathrm{T}} \left(\frac{2}{a} \tilde{\mathbf{\Phi}}^{i}_{\mathrm{u},\xi} t_x + \frac{2}{b} \tilde{\mathbf{\Phi}}^{i}_{\mathrm{u},\eta} t_y \right) \quad 0 \quad 0 \quad 0 \right\} \tag{57}$$

The last term to be determined is the kinetic energy of the stiffener, whose expression is given by Eq. (40). Recalling Eqs. (41), (42) and (44), the Ritz approximation is:

$$K^i = \frac{1}{2} \mathbf{a}^{\mathrm{T}} \int_{-1}^{1} \begin{bmatrix} \mathbf{\Phi}_{\mathrm{u}}^{\mathrm{T}} \mathbf{R}^{\mathrm{T}} \mathbf{M}_{\mathrm{uu}} \mathbf{R} \mathbf{\Phi}_{\mathrm{u}} & \mathbf{\Phi}_{\mathrm{u}}^{\mathrm{T}} \mathbf{R}^{\mathrm{T}} \mathbf{M}_{\mathrm{u}\theta} \mathbf{R} \boldsymbol{\mathcal{J}}^{\mathrm{T}} \mathbf{\Phi}_{\theta} \\ \mathbf{\Phi}_{\theta}^{\mathrm{T}} \boldsymbol{\mathcal{J}} \mathbf{R}^{\mathrm{T}} \mathbf{M}_{\theta\mathrm{u}} \mathbf{R} \mathbf{\Phi}_{\mathrm{u}} & \mathbf{\Phi}_{\theta}^{\mathrm{T}} \boldsymbol{\mathcal{J}} \mathbf{R}^{\mathrm{T}} \mathbf{M}_{\theta\theta} \mathbf{R} \boldsymbol{\mathcal{J}}^{\mathrm{T}} \mathbf{\Phi}_{\theta} \end{bmatrix} J_{\mathrm{s}} \, \mathrm{d}p \, \ddot{\mathbf{a}} = \frac{1}{2} \mathbf{a}^{\mathrm{T}} \mathbf{M}^i \ddot{\mathbf{a}} \tag{58}$$

2.7. Stiffened panel governing equations

The set of discrete governing equations for the stiffened panel can be derived after substitution of the energy terms derived in the preceding sections into Eq. (1) and by application of the stationarity condition of Eq. (5). The final equations are obtained in the form:

$$\left(\mathbf{K} + \beta_2 \lambda \mathbf{K}_{\mathrm{g}} - \beta_3 \omega^2 \mathbf{M} \right) \mathbf{a} = \beta_1 \mathbf{F} \tag{59}$$

where $\mathbf{K}$, $\mathbf{K}_{\mathrm{g}}$ and $\mathbf{M}$ are the assembled stiffness, geometric stiffness and mass matrices of the stiffened panel, while $\mathbf{F}$ is the vector of the external loads.

It is worth noting that the assembly of the terms entering Eq. (59) is particularly straightforward, as far as plate/stiffener compatibility conditions are enforced in strong-form manner (see Eq. (32)). It follows that the stiffened-panel's assembled matrices are available by summing the various contributions as:

$$\mathbf{K} = \breve{\mathbf{K}} + \sum_{i=1}^{\mathrm{N_s}} \mathbf{K}^i \qquad \mathbf{K}_{\mathrm{g}} = \breve{\mathbf{K}}_{\mathrm{g}} + \sum_{i=1}^{\mathrm{N_s}} \mathbf{K}_{\mathrm{g}}^i \quad \mathbf{M} = \breve{\mathbf{M}} + \sum_{i=1}^{\mathrm{N_s}} \mathbf{M}^i \tag{60}$$

and:

$$\mathbf{F} = \breve{\mathbf{F}}_{\mathrm{u}} + \breve{\mathbf{F}} + \sum_{i=1}^{\mathrm{N_s}} \mathbf{F}_{\mathrm{u}}^{i} + \mathbf{F}^{i} \tag{61}$$

Referring to Eq. (59) and Table 1, it can be gleaned that a static analysis implies the solution of a linear system, while a free-vibration problem requires the solution of an eigenvalue problem. On the contrary, buckling analyses and pre-stressed free-vibration problems require a two-step procedure, where the linear static problem is solved first to determine $\mathbf{K}_{\mathrm{g}}$, and the resulting eigenvalue problem is solved in a second step.

In most cases, a reduced number of degrees of freedom is needed to guarantee converged solutions, therefore the solution of Eq. (59) is carried out in a highly efficient way. It is worth mentioning that the assembled matrices are generally fully populated as a result of the numerical integration process, which is necessary when variable-stiffness configurations are of concern. In the particular case of composite panels with straight fiber orientations, the Ritz integrals can be carried out analytically, leading to an increased degree of sparsity of the assembled matrices, with beneficial effects on the time required for the solution.

3. Results

In this section, the semi-analytical formulation is applied to the analysis of different test cases aimed at demonstrating the capabilities of the present modeling strategy. The results are presented for VS panels of increasing level of complexity: starting from unstiffened plates, the analyses are then presented for stiffened panels with straight and curvilinear stiffeners. The panels investigated in the section are made of typical aerospace carbon/epoxy materials, whose thermo-elastic properties

are summarized in Table 3. Free-vibration, with or without pre-stresses, mechanical and thermal buckling problems are considered. The comparisons are illustrated against results from the literature, obtained using different numerical techniques. The computations are conducted by retaining the same number of terms for all the displacement components and the corresponding expansion is indicated as $R \times S$. The number of functions is specified from case to case on the basis of preliminary convergence tests, while the number of integration points, unless otherwise specified, is taken to be equal to $R+5$ and $S+5$ for the directions ξ and η, respectively. Line integrals are performed using $R+S+5$ points, this choice motivated by a set of preliminary studies.

3.1. Unstiffened panels

Example 1: Pre-buckling and buckling analysis

The first example deals with the analysis of the elastic instability of a VS unstiffened plate, previously studied by Wu et al. [6]. The plate is square and has side dimension equal to 254 mm, while the material properties are those of Mat A in Table 3. The stacking sequence is in the form $[\pm\theta_1/\pm\theta_2]_{\mathrm{s}}$ with a non-linear fiber orientation varying according to Eq. (6). The fiber paths were determined in Ref. [43] to maximize the buckling load under compression, and the corresponding stacking sequences are summarized in the Appendix for three designs. The first one is based on a fiber variation along the y direction, while the second and third lay-ups consider a non-linear law prescribed by means of a grid of three and five points, respectively. The load is introduced through the end shortening of the two parallel edges at x=const, while the two others are free to deform. Simply-supported conditions are assumed at the four edges, where rotations around the axis normal to

edges are set to zero, consistently with the thin-plane formulation of Ref. [6]. A point constraint is introduced in the form of a penalty term to avoid stiffness matrix singularity when solving the pre-buckling problem. A number of 15 functions along both directions was found as adequate for guaranteeing convergence of the results, which are reported in terms of the nondimensional buckling coefficient $\breve{K}_{\rm cr} = \breve{N}_{xx}^{\rm cr} \dfrac{a^2}{E_{11} t^3}$, where:

$$\breve{N}_{xx}^{\rm cr} = \frac{1}{b} \lambda \int_{-b/2}^{b/2} N_{xx}|_{x=\pm a/2} \, {\rm d}y \tag{62}$$

is the average axial force per unit length, while $N_{xx} = N_{xx}(x, y)$ is evaluated in a post-processing phase, after introducing the constitutive law and differentiating the displacement components. In this regard, it is noted that highest accuracy was found by performing the integral of Eq. (62) not exactly at the edge, but in correspondence of the first integration point of the in-plane integration scheme.

The distribution of pre-buckling membrane resultants is shown in Figure 4, and the comparison is presented against the results obtained by Wu et al. [6] using a Ritz approach formulated in terms of stress function. For consistency with reference results, the values are scaled to achieve a unitary maximum value for N_{xx}, corresponding to an axial shortening of 1.6×10^{-3} mm. Similarly, the force resultants are taken positive in compression. The contour plot in the figure reveals the good quality of the pre-buckling predictions, which confirms the validity of the linear static formulation. The patterns of the membrane forces are highly similar, and the slight discrepancies observed can be ascribed to different visualization of the plots.

The buckling values of the first two modes are reported in Table 4 along with Ritz and Abaqus finite element calculations from Ref. [6]. The first two eigenvalues are almost coincident in all the cases, as typical for VS plates designed to maximized the buckling load. Excellent agreement is obtained for the three designs, with maximum

percent differences, calculated with respect to the FE results, of approximately 0.5%.

3.2. Stiffened panels with straight stiffeners

Example 2: Buckling analysis and pre-stressed vibrations

The example proposed by Zhao and Kapania [36] is considered to illustrate the case of a stiffened panel with variable-stiffness skin.

The panel is square, with dimension of 300 mm, and is made of Mat A, whose density is 1800 kg/m^3. The skin is obtained by the stacking of 8 plies of thickness 0.1272 mm and oriented at $[\pm\theta]_{2s}$. The variation of the fiber orientation is obtained by assigning the orientation angles in a grid of 3×3 points, as reported in the Appendix. Two equally spaced stiffeners of Mat A, having height equal to $5t$ and obtained by the stacking of 8 plies at 0 degrees, are located at $y = \pm b/6$. They are assumed to be symmetrically located with respect to the skin midplane, thus the effects due to eccentricity are not accounted for. The edges are free to deform along their tangential direction, while they are prevented from the motion along the normal direction, when this latter is not prescribed. Different sets of flexural boundary conditions are accounted for, namely SSSS, SCSC and CCCC (the order of the edges is available from Figure 1). Note, a simply-supported edge is intended here to prevent out-of-plane displacement only, while no constraints are introduced regarding the two rotation components. All simulations are performed using an expansion of 20×20 functions.

Firstly, the buckling response is investigated by considering a uniform compression imposed by means of a prescribed end shortening at the two edges at $x = \pm a/2$. The pre-buckling stress distribution is illustrated in Figure 5 for the fully-clamped panel, where the comparison is presented with the results derived by Zhao and Kapania [36] using a finite element approach. It is noted that reference finite element models

are realized using shell elements for the skin and beam elements for the stiffeners. Therefore, they provide a comparison in terms of equivalent structural idealization of the panel components, and any difference can be ascribed to the numerical solution strategy of the problem. As seen, the agreement is close, showing the ability of the present Ritz approach to capture even relatively complex patterns. The membrane stress gradients are relatively strong, but the good convergence properties of Legendre polynomials allow this behavior to be well-represented. The panel was designed to maximize the buckling response, therefore the typical mechanism of stress redistribution toward the edges is clearly observed when examining the membrane stress N_{xx}.

The buckling results are summarized in Table 5 for the three sets of boundary conditions at hand. The nondimensional buckling load accounts for the contributions carried by the skin and the stiffeners, and is expressed as:

$$K_{\text{cr}} = \lambda \left(\breve{N}_{xx}^{\text{cr}} + \frac{1}{b} \sum_{i=1}^{2} P^i \right) \frac{a^2}{E_{11} t^3} \tag{63}$$

where $\breve{N}_{xx}^{\text{cr}}$ is defined by Eq. (62), and P^i is the axial force carried by the stiffeners. The results of Table 5 reveal good agreeent even in terms of buckling loads, the maximum percent different being close to 2% in the SCSC case, while it is less than 1% for the two other sets of boundary conditions.

The same panels are analyzed in terms of free-vibration response in the presence of a pre-stress state. Specifically, the load is initially introduced by prescribing the axial displacement, measured as a fraction of that of a quasi-isotropic skin configuration with lay-up $[\pm 45/0/90]_{\text{s}}$ and free to deform laterally. For the three set of boundary conditions considered here, the critical displacements are 0.021 mm, 0.031 mm and 0.059 mm, respectively.

The dimensional frequencies are compared with those reported in Ref. [36] in Table 6. As shown, the Ritz predictions are accurate and closely resemble those obtained using finite elements, the maximum difference being well below 2%.

3.3. Stiffened panels with curvilinear stiffeners

Example 3: Buckling analysis and pre-stressed vibrations

Results are now presented for panels stiffened by curvilinear stiffeners. The literature in this field is relatively scarce, but useful results to be used as a benchmark can be found in Ref. [36]. Square panels of dimension 300 mm are considered. The material for the skin and the stiffeners is the one denoted as Mat A in Table 3. The skin lay-up has sequence $[\pm\theta_1/\pm\theta_2]_{2s}$, corresponding to 16 plies and a total thickness of 2.032 mm. The four curvilinear stiffeners are characterized by a width equal to the skin thickness, and a five-times-larger height. All the plies are oriented at 0 degrees. The stiffener paths are taken from Ref. [36], where the parameterization is performed using Hobby splines. A minimum least square fitting is performed in order to transform the paths into the third-order Bézier description implemented in the present formulation. For completeness, the coordinates of the so obtained control points are provided in the Appendix.

Simply-supported boundary conditions are assumed, with the four edges prevented from out-of-plane displacements, but free to rotate. The transverse edges are constrained along the normal direction, thus any expansion or contraction is prevented. Consistently with Ref. [36], the buckling results are presented in terms of buckling multipliers associated with a pre-buckling axial shortening of 0.02 mm in Table 7. This implies that buckling displacements are available as the product between 0.02 mm and the values in the table. Computations are conducted with and without

accounting for the stiffener eccentricity.

Given the relatively complex configuration of the panel under investigation, it is interesting to illustrate a preliminary convergence study – see Table 7 – with respect to the predicted first buckling eigenvalue. The goal of the analysis is twofold. Firstly, motivating the choice for the number of functions used in subsequent analyses; secondly, highlighting the difference of requirements between pre-buckling and buckling analysis. A grid of 30 integration points is considered, irrespective of the number of trial functions, so that the number of points remains larger than the order of the expansions considered in the table. In the present analysis, the solution is referred to as converged when two successive analyses differ from each other by less than 1%. The number of trial functions is reported in Table 7 with respect to the pre-buckling and the buckling analyses. In particular, the convergence of the pre-buckling solution can be inspected moving along the rows of the table, while that of the buckling solution is available by moving along the column-wise direction. As shown, faster convergence is observed for pre-buckling than for buckling. The pre-buckling problem is essentially a membrane problem – slight bending effects exist due to stiffener eccentricity, but their role is not primary –, and the presence of stress gradients, due to continuous skin stiffness variability, is relatively straightforward to capture. Therefore, adding more than 15 functions has no effect on the buckling prediction. More functions are needed for solving the buckling problem. Specifically, R has to be taken equal to 20 and 25 in the concentric and eccentric case, respectively. As a matter of fact, the buckled shape can be more difficult to represent, especially when the presence of stiffeners is responsible for the onset of local buckles. Owing to the requirements outlined previously, the solution of the problem can be optimized in terms of computational efficiency, and the two steps for the buckling prediction can

be performed by considering different numbers of degrees of freedom. It is emphasised that the required enlargement of the basis for the buckling analysis does not demand a full re-computation of the stiffness matrix, but just the additional terms need to be evaluated. This is a peculiar aspect of the Ritz method, which can not be exploited in the context of a finite element procedure.

The comparison against reference results (see Table 7) reveals that close agreement is obtained with the finite element technique proposed in Ref. [36], as well as with NASTRAN predictions. These conclusions hold for both the concentric and eccentric cases, demonstrating that the effect due to the stiffener eccentricity is correctly captured. It can be noted that larger predictions are obtained, for some results, with respect to the FEM ones, while in others they are smaller. The same is true referring to the NASTRAN values. This behavior is explained by the non-monotonic convergence of the three numerical techniques in the table, primarily due to the discretization of the fiber path. Furthermore, the path of the stiffeners considered here is not exactly the same as the reference models due to different spline descriptions, which leads to small, but non-null, source of errors. However, the quality of the predictions is good, and reveals the ability of the present approach to effectively handle the case of curvilinear stiffeners. The comparison of the first two buckled shapes is provided in Figure 6 in terms of contour plots of the out-of-plane deflections. In all cases, the modes are of global type, with stringers lifting from the surface and undergoing bending deformation. However, interactions with localized buckles is noted when eccentricity effects are accounted for, which explains the stricter requirements in terms of trial functions observed from Table 7. It is interesting to highlight the difference of the buckled shapes with or without accounting for the stiffener eccentricity: the first mode is characterized by one single half-wave along both directions

when $e = 0$, while a local buckle is observed for $e \neq 0$. This effect is mainly driven by the different pre-buckling stress distributions – eccentric stiffeners promote pre-buckling out-of-plane deflections, and alter the pre-stress distribution in the skin and the stiffeners –, and is confirmed by the free-vibration analysis presented next. In particular, the same panel is studied with regard to its free-vibration response, and the pre-stress state induced by a 0.02 mm compressive displacement is introduced. The first ten frequencies are summarized in Table 8, while the first two eigenmodes are plotted in Figure 7. Converged results are achieved by taking $R = 20$, as localization effects are milder with respect to the buckling case. Again, the comparison against the results of Ref. [36] demonstrates the capabilities of the present approach to appropriately capture the expected response. Very good accuracy can be noticed in terms of predicted frequencies as well as modal shapes. In this case, the pre-stresses play a minor role, as the 0.02 mm prescribed displacement corresponds to 1/10 of the buckling shortening, approximately. Therefore, the main distinction between concentric and the eccentric cases is to be identified in the different bending stiffness of the stringers with respect to the panel midplane. As shown, this effect itself does not promote the drastic change of modal shape observed in the buckling analysis (see Figures 6 and 7).

To complete the discussion of results, it is useful to highlight the computational advantages of the present formulation. In particular, one useful metric to consider is given by the number of degrees of freedom involved for the solution of the problem. In the two examples just considered, R was taken equal to 25 and 20, leading to problem sizes of 2400 and 3750, respectively. The comparison with a similar strategy based on a FE approach can be performed by considering the mesh used for obtaining the results reported in Ref. [36], previously used for the comparison. They

are based on 32×32 biquadratic elements with eight nodes, leading to a number of degrees of freedom which is, approximately, 6 to 10 times higher. It is useful to present the computational times for constructing the stiffness matrix for the examples at hand, which is the most critical aspect from an implementation perspective. As a matter of fact, the surface integrals of the present Ritz formulation must be carried out numerically due to the planar variability of the laminate's elastic coefficients. This operation can restrict the maximum number of trial functions that can be used due the time needed to perform the integrals. Specifically, the current – yet not optimized – version of the Matlab code implementing the formulations leads to CPU times (on a standard PC with Intel i7 Core, 4.00 GHz, 32 GB RAM) of, approximately, 0.25, 2, 10 and 30 s when the number of functions is taken as 10×10, 15×15, 20×20, 25×25, respectively. One can observe that the computational time tends to diverge if the expansion is raised up to several tens of functions. However, in most cases of practical interest, a maximum number of 20 to 25 functions suffices for achieving accurate results and, in these cases, the total time is relatively small. Also, it should be noted that the matrices obtained using the present formulation do not offer the matrix band structure and the sparsity typical of FEM, although the orthogonality properties of Legendre polynomials tend to guarantee a non negligible degree of sparsity – in this example the number of not-null terms is around 30%. Irrespective on this, the significantly smaller dimensions of the problem balance the mentioned disadvantages, leading to an overall attractive computational effectiveness of the method. These considerations are even more noteworthy when straight-fiber configurations are analyzed, as far as in-plane integrals can be conducted analytically, and high matrix sparsity achieved due to the orthogonality properties of the trial functions employed.

Example 4: Thermal buckling analysis

A final example is discussed to provide a complete overview of the features of the present approach, which include the thermal buckling solver. To meet this aim, the example taken from Ref. [35] is considered. To the best of the authors' knowledge, the referenced one is the only work in the literature concerning thermal buckling of VS panels with curvilinear stiffeners.

The panel is square and has size equal to 150 mm, with material properties of Mat B. The skin is layered by 8 plies of thickness 0.127 mm with orientation $[\pm < 69|-5.705 >]_{2s}$. Therefore, plies are oriented at ± 69 degrees at the panel center, and they rotate linearly with the coordinate x up to ∓ 5.705 at the edges at $x = \pm a/2$. The panel is stiffened by two curvilinear stringers with height 5.08 mm, and obtained by the stacking of 8 plies at 0 degrees. The stiffener paths, which are taken from the Hobby spline description of Ref. [35], are converted into a Bézier-type representation using a minimum least-square fitting approach. The coordinates of the control points are provided in the Appendix. A uniform temperature increase ΔT is considered, with the panel prevented from in-plane motion at the four edges. Flexural boundary conditions are of simply-support type, with out-of-plane deflections set to zero and rotation components left free along the overall boundary.

The first ten critical temperatures are reported in Table 9 and the first two buckled shapes are depicted in Figure 8. The comparison is taken against the finite element results of Ref. [35], based on a mesh of 24 8-node elements, and leading to a problem size 5 to 6 times greater than the present approach. Indeed preliminary analyses, not reported here for the sake of brevity, revealed that 20×20 functions provide converged results. Indeed, the presence of just two stringers avoids the onset of highly localized modes, as seen from Figure 8.

The agreement with the finite element strategy developed by Zhao and Kapania [35] is satisfying, the maximum difference between predicted and reference eigenvalues being smaller than 1.5% in the worst cases, and well below 0.5% in the vast majority of cases. Close similarity is revealed even in terms of buckled mode shape. As discussed previously, a clear distinction exists between concentric and eccentric stiffeners, the latter responsible for higher buckling loads.

4. Conclusions

A novel semi-analytical strategy for the analysis of stiffened panels characterized by VS skin and curvilinear stringers has been introduced and presented. The approach relies on the combined use of first-order theories for the plate and beam elements, along with the Ritz method for seeking an approximate solution.

The formulation has been developed for several solution procedures, including static, free-vibration, buckling and thermal-buckling analyses. A wide set of design conditions is guaranteed by accounting for different boundary and loading conditions. In the examples presented, orientation angles are described by using Lagrange polynomials, which allowed to replicate results from the literature. Other representations – Legendre polynomials or Chebyshev points – are possible, and this can be particularly useful to prevent Runge effects when orientation angles are prescribed at several points.

The main goal of the study was to illustrate the approach, comparing the results against the few available in the literature, especially for the variable-stiffness case. In this regard, different test cases were discussed, demonstrating the validity of the proposed formulation and the accuracy of the predictions.

One of the main advantages of the method is that no mesh needs to be generated.

This is particularly convenient when the stiffeners are not straight, as the generation of finite element models requires special care to enforce skin/stiffener continuity. Furthermore, the arbitrary fiber paths can be defined straightforwardly, thus the analysis of panels characterized by VS skins is particularly straightforward to pursue. The use of the present formulation is thus suggested in the context of preliminary studies and optimizations for innovative configurations characterized by VS skins and curvilinear stiffeners.

The results illustrate that requirements in terms of degrees of freedom are influenced by the number of stiffeners, as they may trigger local modes, and, in turn, improved spatial descriptions are required. However, the choice of Legendre polynomials allows large sets of functions to be considered with relative ease with no observable stability or numerical issues. In the cases presented, polynomials up to the order of 25 were considered, and proved to be capable of capturing difficult to model, highly localized modes. Overall, the number of degrees of freedom tends to be much smaller when compared to finite element models with similar accuracy, suggesting the adoption of the present strategy as a robust alternative to finite elements.

References

[1] M.W. Hyer and R.F. Charette. Use of curvilinear fiber format in composite structure design. *AIAA Journal*, 29(6):1011–1015, 1991.

[2] R. Olmedo and Z. Gürdal. Buckling response of laminates with spatially varying fiber orientations. In 34^{th} *AIAA/ASME/ASCE/AHS/ASC Structures, Structural Dynamics and Material Conference*, La Jolla, CA, April 19–22 1993.

[3] B.F. Tatting and Z. Gürdal. Analysis and design of tow-steered variable stiffness composite laminates. In *AHS Meeting*, Williamsburg, VA, 30 October–1 November 2001.

[4] Z. Gürdal, B.F. Tatting, and C.K. Wu. Variable stiffness composite panels: effects of stiffness variation on the in-plane and buckling response. *Composites Part A: Applied Science and Manufacturing*, 39(5):911–922, 2008.

[5] T. Rahman, S.T. Ijsselmuiden, M.M. Abdalla, and E. Jansen. Postbuckling analysis of variable stiffness composite plates using a finite element-based perturbation method. *International Journal of Structural Stability and Dynamics*, 11(4):735–753, 2011.

[6] Z. Wu, P.M. Weaver, G. Raju, and B.C. Kim. Buckling analysis and optimisation of variable angle tow composite plates. *Thin-Walled Structures*, 60:163–172, 2012.

[7] Z. Wu, G. Raju, and P.M. Weaver. Postbuckling analysis of variable angle tow composite plates. *International Journal of Solids and Structures*, 50(10):1770–1780, 2013.

[8] G. Raju, Z. Wu, and P.M. Weaver. Buckling and postbuckling of variable angle tow composite plates under in-plane shear loading. *International Journal of Solids and Structures*, 58:270–287, 2015.

[9] B.H. Coburn and P.M. Weaver. Buckling analysis, design and optimisation of variable-stiffness sandwich panels. *International Journal of Solids and Structures*, 96:217–228, 2016.

[10] Z. Wu, G. Raju, and P.M. Weaver. Optimization of postbuckling behaviour of variable thickness composite panels with variable angle tows: towards Buckle-Free design concept. *International Journal of Solids and Structures*, 132:66–79, 2018.

[11] R. Vescovini and L. Dozio. Thermal buckling behaviour of thin and thick variable-stiffness panels. *Journal of Composites Science*, 2(4):1–23, 2018.

[12] G. Manickam, A. Bharath, A.N. Das, A. Chandra, and P. Barua. Thermal buckling behaviour of variable stiffness laminated composite plates. *Materials Today Communications*, 16:142–151, 2018.

[13] V. Oliveri, A. Milazzo, and P.M. Weaver. Thermo-mechanical post-buckling analysis of variable angle tow composite plate assemblies. *Composite Structures*, 183:620–635, 2018.

[14] M.M. Abdalla, S. Setoodeh, and Z. Gürdal. Design of variable stiffness composite panels for maximum fundamental frequency using lamination parameters. *Composite Structures*, 81(2):283–291, 2007.

[15] H. Akhavan and P. Ribeiro. Natural modes of vibration of variable stiffness composite laminates with curvilinear fibers. *Composite Structures*, 93(11):3040–3047, 2011.

[16] S. Yazdani and P. Ribeiro. A layerwise p-version finite element formulation for free vibration analysis of thick composite laminates with curvilinear fibres. *Composite Structures*, 120:531–542, 2015.

[17] C. Lopes, P.P. Camanho, and Z. Gürdal. Progressive failure analysis of tow-placed, variable-stiffness composite panels. *International Journal of Solids and Structures*, 44(25-26):8493–8516, 2007.

[18] V. Oliveri and A. Milazzo. A Rayleigh-Ritz approach for postbuckling analysis of variable angle tow composite stiffened panels. *Computers & Structures*, 196:263–276, 2018.

[19] R. Vescovini and L. Dozio. A variable-kinematic model for variable stiffness plates: Vibration and buckling analysis. *Composite Structures*, 142:15–26, 2016.

[20] Z. Wu, G. Raju, and P.M. Weaver. Framework for the buckling optimization of variable-angle tow composite plates. *AIAA Journal*, 53(12):3788–3804, 2015.

[21] Z. Gürdal and B. Grall. Buckling analysis of geodesically stiffened composite panels with discrete stiffeners. *Journal of Aircraft*, 31(5):1197–1204, 1994.

[22] R.K. Kapania, J. Li, and H. Kapoor. Optimal design of unitized panels with curvilinear stiffeners. In *AIAA* 5^{th} *Aviation, Technology, Integration, and Operations Conference (ATIO)*, AIAA 2005-7482, Arlington, VA, 26–28 September 2005.

[23] P. Joshi, S. Mulani, R.K. Kapania, and Y. Shin. Optimal design of unitized structures with curvilinear stiffeners using response surface methodology. In 49^{th} *AIAA/ASME/ASCE/AHS Structures, Structural Dynamics and Material Conference*, AIAA 2008-2304, Schaumburg, IL, April 7–10 2008.

[24] S.P. Gurav and R.K. Kapania. Development of framework for the design optimization of unitized structures. In 50^{th} *AIAA/ASME/SAE Structures, Structural Dynamics and Materials Conference*, AIAA 2009-2186, Palm Springs, CA, May 4–7 2009.

[25] D. Locatelli, S.B. Mulani, Q. Li, A.Y. Tamijani, and R.K. Kapania. Supersonic wing optimization using SpaRibs. CR 218537, NASA, 2014.

[26] P. Shi, R.K. Kapania, and C.Y. Dong. Vibration and buckling analysis of curvilinearly stiffened plates using finite element method. *AIAA Journal*, 53(5):1319–1335, 2015.

[27] W. Zhao and R.K. Kapania. Buckling analysis of unitized curvilinearly stiffened composite panels. *Composite Structures*, 135:365–382, 2016.

[28] W. Zhao and R.K. Kapania. Vibration analysis of curvilinearly stiffened composite panel subjected to in-plane loads. *AIAA Journal*, 55(3):981–997, 2017.

[29] A.Y. Tamijani and R.K. Kapania. Vibration of plate with curvilinear stiffeners using mesh-free method. *AIAA Journal*, 48(8):1569–1581, 2010.

[30] A.Y. Tamijani and R.K. Kapania. Buckling and static analysis of curvilinearly stiffened plates using mesh-free method. *AIAA Journal*, 48(12):2739–2751, 2010.

[31] A.Y. Tamijani and T. McQuigg R.K. Kapania. Free vibration analysis of curvilinear-stiffened plates and experimental validation. *Journal of Aircraft*, 47(1):192–200, 2010.

[32] A.Y. Tamijani and R.K. Kapania. Chebyshev-Ritz approach to buckling and vibration of curvilinearly stiffened plate. *AIAA Journal*, 50(5):1007–1018, 2010.

[33] R. Fernandes and A.Y. Tamijani. Flutter analysis of laminated curvilinear-stiffened plates. *AIAA Journal*, 55(3):998–1011, 2017.

[34] K. Singh and R.K. Kapania. Optimal design of tow-steered composite laminates with curvilinear stiffeners. In *2018 AIAA/ASCE/AHS/ASC Structures, Structural Dynamics, and Materials Conference*, AIAA 2018-2243, Kissimmee, FL, 8–12 January 2018.

[35] W. Zhao, K. Singh, and R.K. Kapania. Thermal buckling analysis and optimization of curvilinearly stiffened plates with variable angle tow laminates. *Journal of Spacecraft and Rockets*, pages 1–16, 2019.

[36] W. Zhao and R.K. Kapania. Prestressed vibration of stiffened variable-angle tow laminated plates. *AIAA Journal*, pages 1–19, 2019.

[37] A. Milazzo and V. Oliveri. Post-buckling analysis of cracked multilayered composite plates by pb-2 Rayleigh–Ritz method. *Composite Structures*, 132:75–86, 2015.

[38] R. Vescovini, L. Dozio, M. D'Ottavio, and O. Polit. On the application of the Ritz method to free vibration and buckling analysis of highly anisotropic plates. *Composite Structures*, 192:460–474, 2018.

[39] K.M. Liew and C.M. Wang. pb-2 Rayleigh-Ritz method for general plate analysis. *Engineering Structures*, 15(1):55–60, 1993.

[40] J.N. Reddy. *Mechanics of Laminated Composite Plates and Shells: Theory and Analysis*. CRC Press, Boca Raton, 2004.

[41] L. Martini and R. Vitaliani. On the polynomial convergent formulation of a C^0 isoparametric skew beam element. *Computers & Structures*, 29(3):437–449, 1988.

[42] Z. Wu, G. Raju, and P.M. Weaver. Comparison of variational, differential quadrature, and approximate closed-form solution methods for buckling of highly flexurally anisotropic laminates. *Journal of Engineering Mechanics*, 139(8):1073–1083, 2012.

[43] S. IJsselmuiden, M.M. Abdalla, and Z. Gürdal. Optimization of variable-stiffness panels for maximum buckling load using lamination parameters. *AIAA Journal*, 48(1):134–143, 2010.

[44] J.C. Massa and E.J. Barbero. A strength of materials formulation for thin walled composite beams with torsion. *Journal of Composite Materials*, 32(17):1560–1594, 1998.

Table 1: Scalar coefficients of the energy function for different analysis types.

Analysis	β_1	β_2	β_3
static	1	0	0
buckling	0	1	0
free-vibration	0	0	1
pre-stressed free-vibration	0	1	1

Table 2: Coefficients of the boundary functions.

Position	Free	Fixed
ξ=1	$a_1 = 0$	$a_1 = 1$
ξ=-1	$a_2 = 0$	$a_2 = 1$
η=1	$a_3 = 0$	$a_3 = 1$
η=-1	$a_4 = 0$	$a_4 = 1$

Table 3: Material thermo-elastic properties.

	Mat A	Mat B
E_{11} (MPa)	181000	147000
E_{22} (MPa)	10270	10300
G_{12} (MPa)	7170	7000
G_{13} (MPa)	4000	7000
G_{23} (MPa)	4000	7000
ν_{12}	0.28	0.27
α_{11} (1/°C)	/	-0.9$\times 10^{-6}$
α_{22} (1/°C)	/	27$\times 10^{-6}$

Table 4: Nondimensional buckling parameter $\breve{K}_{\rm cr}$ for simply-supported unstiffened VS plates under prescribed axial shortening.

Design n.	Mode n.	Ritz ([6])	FEM ([6])	Ritz (15×15)
1	1	3.4991	3.4990	3.5209
	2	3.5026	3.5058	3.5250
2	1	3.7112	3.6750	3.6865
	2	3.7227	3.6973	3.7075
3	1	3.7849	3.7341	3.7558
	2	3.8054	3.7607	3.7822

Table 5: Nondimensional buckling parameter K_{cr} for VS panels stiffened by two straight stiffeners under prescribed axial shortening.

	FEM ([36])	Ritz (20×20)
SSSS	2.88	2.87
SCSC	4.68	4.79
CCCC	9.55	9.64

Table 6: Dimensional frequencies (Hz) with and without pre-stress for VS panels stiffened by two straight stiffeners.

	FEM ([36])				Ritz (20×20)			
$\Delta\overline{u}/\Delta\overline{u}^{\mathrm{qi}} =$	0	0.1	0.5	1.0	0	0.1	0.5	1.0
SSSS	90.71	87.99	80.62	73.10	90.89	87.84	80.36	74.22
SCSC	135.36	133.79	128.58	122.66	135.58	133.80	128.53	122.58
CCCC	193.50	189.17	176.21	161.94	194.91	186.79	177.74	162.80

Table 7: Buckling multipliers for simply-supported VS panels with four curvilinear stringers under prescribed axial shortening of 0.02 mm. Convergence analysis using $R_{\text{pre}} \times R_{\text{pre}}$ and $R_{\text{buck}} \times R_{\text{buck}}$ functions for the pre-buckling and buckling analysis, respectively.

	Concentric ($e = 0$)					Eccentric ($e \neq 0$)				
	R_{buck}					R_{buck}				
R_{pre}	5	10	15	20	25	5	10	15	20	25
3	8.70	7.68	7.50	7.46	7.44	23.78	17.89	17.24	17.06	16.96
5	8.82	7.69	7.49	7.45	7.43	24.82	16.79	16.23	16.06	15.96
10	8.92	7.61	7.40	7.35	7.33	25.57	15.57	14.96	14.79	14.70
15	8.94	7.62	7.41	7.36	7.34	25.65	15.53	14.92	14.75	14.66
20	8.95	7.63	7.42	7.37	7.35	25.67	15.53	14.92	14.75	14.66
25	8.95	7.63	7.42	7.37	7.35	25.68	15.53	14.92	14.75	14.66
FEM ([36]) - NASTRAN ([36])					7.09 - 7.29					14.70 - 14.91

Table 8: Dimensional frequencies (Hz) for pre-stressed simply-supported VS panels with four curvilinear stringers.

	Concentric ($e = 0$)			Eccentric ($e \neq 0$)		
Mode	FEM ([36])	NASTRAN ([36])	Ritz 20×20	FEM [36]	NASTRAN ([36])	Ritz 20×20
1	202.163	204.34	207.74	343.42	336.41	343.76
2	472.458	477.47	493.78	740.61	720.39	750.24
3	514.900	522.25	535.08	795.61	769.60	802.69
4	758.249	768.16	778.24	956.78	952.67	970.32
5	861.464	875.25	894.74	1150.51	1148.54	1153.41
6	1015.298	1033.14	1058.01	1236.34	1245.01	1268.39
7	1113.045	1126.36	1130.76	1345.99	1319.14	1367.69
8	1223.402	1244.45	1260.25	1563.75	1549.75	1590.68
9	1323.388	1354.80	1381.01	1641.03	1629.65	1659.12
10	1149.591	1512.27	1521.03	1694.96	1684.19	1701.95

Table 9: Critical temperatures ($^{\circ}C$) for for simply-supported VS panels with two curvilinear stringers under uniform temperature increase.

	Concentric ($e = 0$)			Eccentric ($e \neq 0$)		
Mode	FEM ([35])	NASTRAN ([35])	Ritz 20×20	FEM [35]	NASTRAN ([35])	Ritz 20×20
1	77.78	78.00	77.89	101.03	100.92	101.83
2	117.44	118.07	118.02	122.61	123.27	123.51
3	138.78	140.06	137.97	150.08	152.25	149.55
4	143.09	144.65	143.04	151.75	153.83	151.13
5	149.92	151.97	149.69	160.01	162.38	160.49
6	159.22	161.87	160.06	165.55	168.37	167.69
7	172.39	175.25	172.55	191.65	196.25	190.97
8	184.28	188.79	184.79	192.01	196.75	192.47
9	192.47	197.64	192.43	205.26	210.70	205.75
10	211.38	216.93	211.99	215.29	222.37	218.01

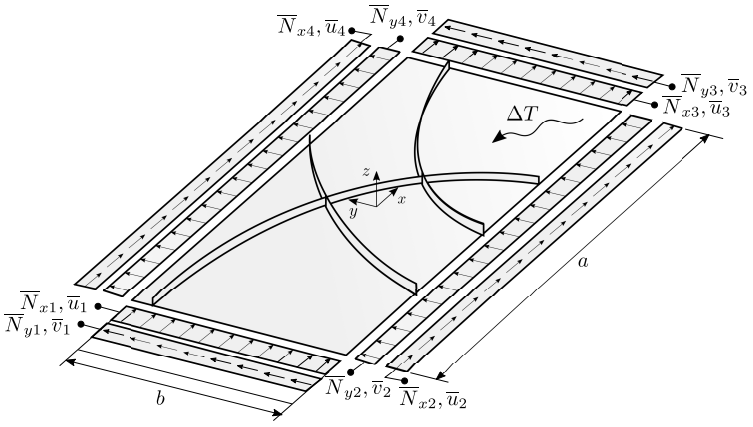

Figure 1: Sketch of a stiffened panel with three curvilinear stringers – dimensions and conventions for edge loads and prescribed displacements.

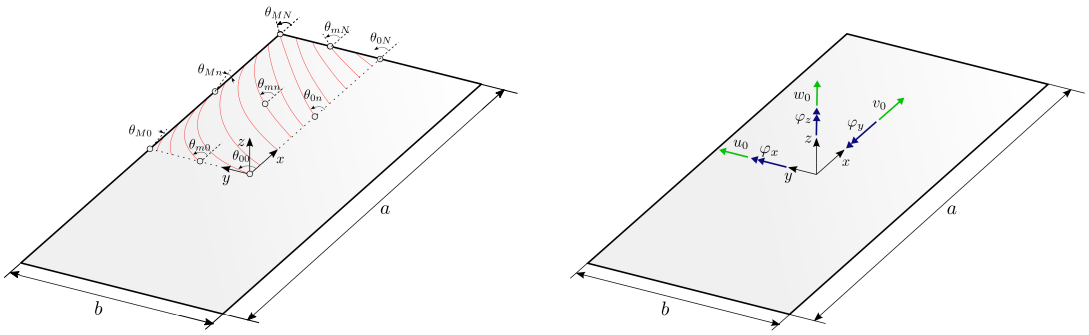

(a) (b)

Figure 2: Plate element: (a) fiber orientation, (b) conventions for generalized displacement components.

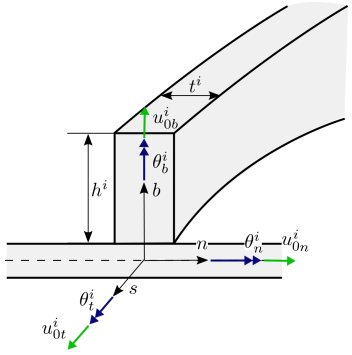

Figure 3: Beam element: dimensions and conventions for generalized displacement components.

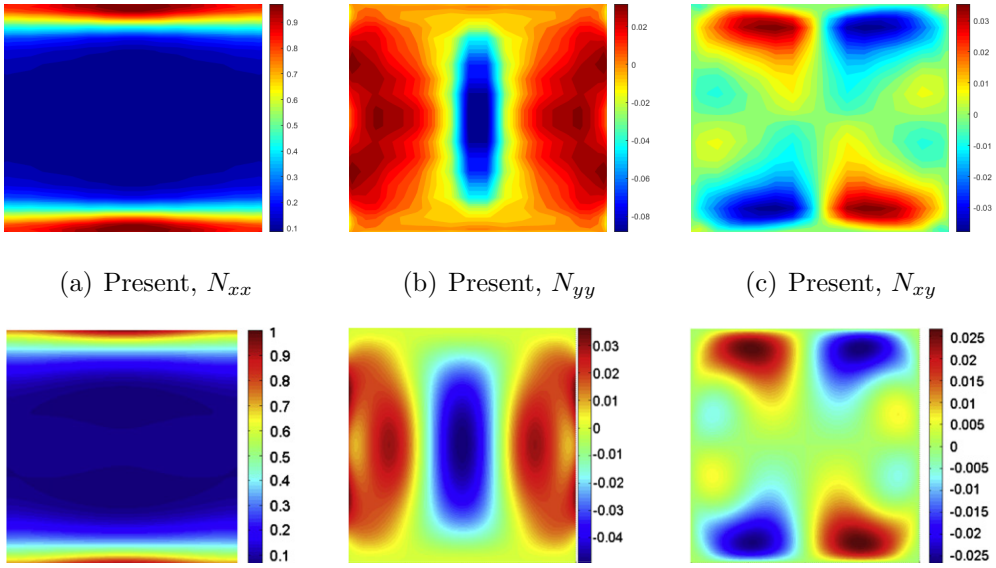

(a) Present, N_{xx} (b) Present, N_{yy} (c) Present, N_{xy}

(d) Ref. [6], N_{xx} (e) Ref. [6], N_{yy} (f) Ref. [6], N_{xy}

Figure 4: Pre-buckling membrane resultants for unstiffened VS plates loaded in compression.

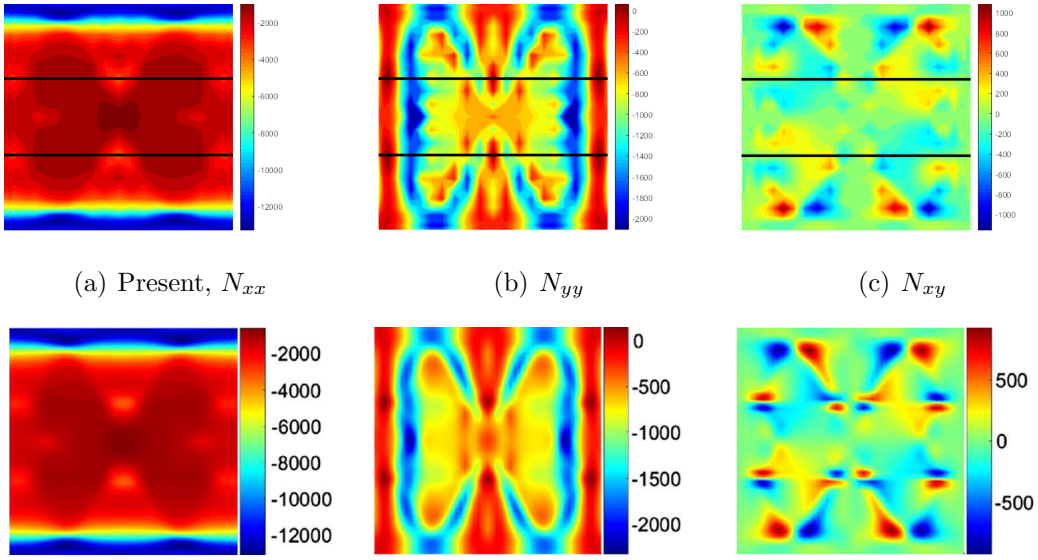

(a) Present, N_{xx} (b) N_{yy} (c) N_{xy}

(d) N_{xx} (e) N_{yy} (f) N_{xy}

Figure 5: Pre-buckling membrane resultants for VS panels stiffened by two straight stiffeners and loaded in compression: (a)-(c) present, (d)-(f) Ref. [36].

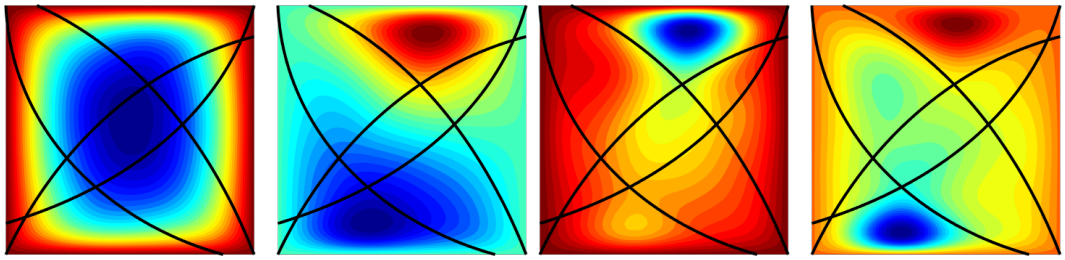

(a) Mode 1, $e = 0$ (b) Mode 2, $e = 0$ (c) Mode 1, $e \neq 0$ (d) Mode 2, $e \neq 0$

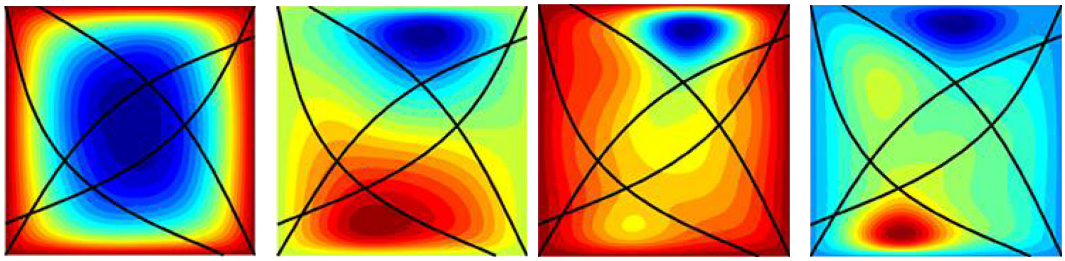

(e) Mode 1, $e = 0$ (f) Mode 2, $e = 0$ (g) Mode 1, $e \neq 0$ (h) Mode 2, $e \neq 0$

Figure 6: Buckling modes for simply-supported VS panels with four curvilinear stringers under prescribed axial shortening: (a)-(d) present, (e)-(h) Ref. [36].

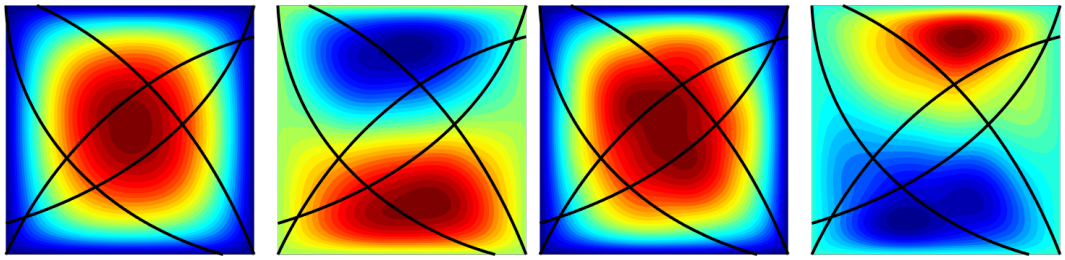

(a) Mode 1, $e = 0$ (b) Mode 2, $e = 0$ (c) Mode 1, $e \neq 0$ (d) Mode 2, $e \neq 0$

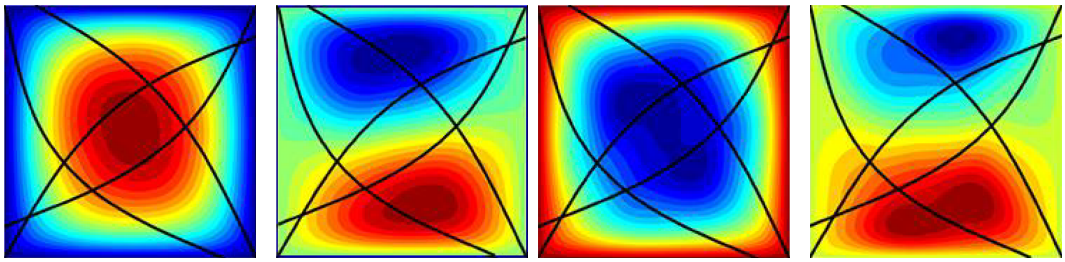

(e) Mode 1, $e = 0$ (f) Mode 2, $e = 0$ (g) Mode 1, $e \neq 0$ (h) Mode 2, $e \neq 0$

Figure 7: Vibration modes for pre-stressed simply-supported VS panels with four curvilinear stringers: (a)-(d) present, (e)-(h) Ref. [36].

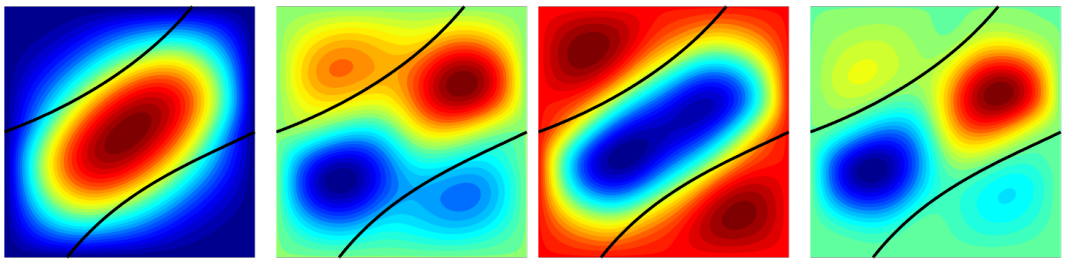

(a) Mode 1, $e = 0$ (b) Mode 2, $e = 0$ (c) Mode 1, $e \neq 0$ (d) Mode 2, $e \neq 0$

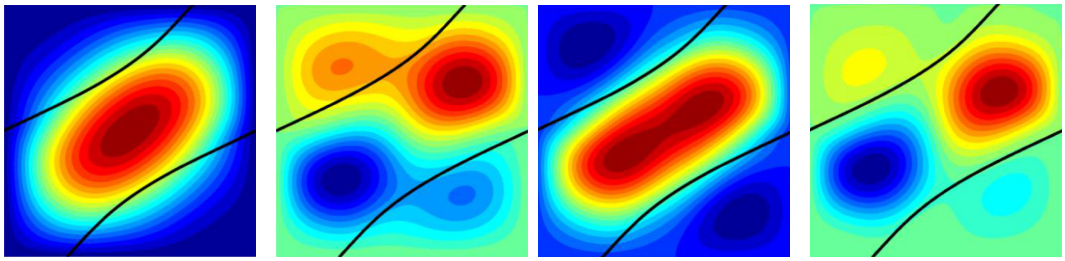

(e) Mode 1, $e = 0$ (f) Mode 2, $e = 0$ (g) Mode 1, $e \neq 0$ (h) Mode 2, $e \neq 0$

Figure 8: Buckling modes for simply-supported VS panels with two curvilinear stringers under uniform temperature increase: (a)-(d) present, (e)-(h) Ref. [35].

5. Appendix

5.1. Differential matrices

$$\boldsymbol{\mathcal{B}}_1 = \begin{bmatrix} (\cdot)_{,x} & 0 & 0 & 0 & 0 & 0 \\ 0 & (\cdot)_{,y} & 0 & 0 & 0 & 0 \\ (\cdot)_{,y} & (\cdot)_{,x} & 0 & 0 & 0 & 0 \\ 0 & 0 & 0 & (\cdot)_{,x} & 0 & 0 \\ 0 & 0 & 0 & 0 & (\cdot)_{,y} & 0 \\ 0 & 0 & (\cdot)_{,x} & 1 & 0 & 0 \\ 0 & 0 & (\cdot)_{,y} & 0 & 1 & 0 \end{bmatrix} \tag{64}$$

$$\boldsymbol{\mathcal{B}}_2 = \begin{bmatrix} 0 & 0 & (\cdot)_{,x} & 0 & 0 & 0 \\ 0 & 0 & (\cdot)_{,y} & 0 & 0 & 0 \end{bmatrix} \tag{65}$$

5.2. Stiffener section properties

A blade stiffener is considered, where the plies are stacked along the stiffener width, i.e. along the direction normal to stiffener height. The stiffener section properties are derived starting from the laminate constitutive law, which is expressed referring to First Order Shear Deformation Theory. Assumptions of specially or-

thotropic stacking sequences are introduced, so:

$$\begin{Bmatrix} N_{xx} \\ N_{yy} \\ N_{xy} \\ M_{xx} \\ M_{yy} \\ M_{xy} \end{Bmatrix} = \begin{bmatrix} A_{11} & A_{12} & 0 & 0 & 0 & 0 \\ A_{11} & A_{12} & 0 & 0 & 0 & 0 \\ 0 & 0 & A_{66} & 0 & 0 & 0 \\ 0 & 0 & 0 & D_{11} & D_{12} & 0 \\ 0 & 0 & 0 & D_{11} & D_{12} & 0 \\ 0 & 0 & 0 & 0 & 0 & D_{66} \end{bmatrix} \left(\begin{Bmatrix} \xi_{xx} \\ \xi_{yy} \\ \xi_{xy} \\ k_{xx} \\ k_{yy} \\ k_{xy} \end{Bmatrix} - \begin{Bmatrix} \hat{\alpha}^i_{xx} \\ \hat{\alpha}^i_{yy} \\ \hat{\alpha}^i_{xy} \\ 0 \\ 0 \\ 0 \end{Bmatrix} \Delta T \right) \tag{66}$$

$$\begin{Bmatrix} Q_y \\ Q_x \end{Bmatrix} = \begin{bmatrix} A^{\mathrm{s}}_{44} & 0 \\ 0 & A^{\mathrm{s}}_{55} \end{bmatrix} \begin{Bmatrix} 2\xi_{yz} \\ 2\xi_{xz} \end{Bmatrix}$$

Assuming that $N^i_{bb} = 0$ and $M^i_{bb} = 0$, Eq. (66) can be inverted to obtain:

$$\begin{Bmatrix} \xi_{xx} \\ 2\xi_{xy} \\ k_{xx} \\ k_{xy} \end{Bmatrix} = \begin{bmatrix} a_{11} & 0 & 0 & 0 \\ 0 & a_{66} & 0 & 0 \\ 0 & 0 & d_{11} & 0 \\ 0 & 0 & 0 & d_{66} \end{bmatrix} \begin{Bmatrix} N_{xx} \\ N_{xy} \\ M_{xx} \\ M_{xy} \end{Bmatrix} + \begin{Bmatrix} \hat{\alpha}^i_{tt} \\ \hat{\alpha}^i_{tb} \\ 0 \\ 0 \end{Bmatrix} \Delta T \tag{67}$$

From which:

$$\begin{Bmatrix} N_{xx} \\ N_{xy} \\ M_{xx} \\ M_{xy} \end{Bmatrix} = \begin{bmatrix} A & 0 & 0 & 0 \\ 0 & F & 0 & 0 \\ 0 & 0 & D & 0 \\ 0 & 0 & 0 & H \end{bmatrix} \left(\begin{Bmatrix} \xi_{xx} \\ \xi_{xy} \\ k_{xx} \\ k_{xy} \end{Bmatrix} - \begin{Bmatrix} \hat{\alpha}^i_{xx} \\ \hat{\alpha}^i_{xy} \\ 0 \\ 0 \end{Bmatrix} \Delta T \right) \tag{68}$$

with:

$$A = \frac{1}{a_{11}} \qquad F = \frac{1}{a_{66}} \qquad D = \frac{1}{d_{11}} \qquad H = \frac{1}{d_{66}} \tag{69}$$

Within the context of the stiffener beam model, the section resultants can be evaluated by integrating the laminate resultants along the blade height:

$$
\begin{aligned}
F_t^i &= \int_h N_{tt}^i \,\mathrm{d}b \;=\; \int_h A\left(\xi_{tt}^i + bk_n - \hat{\alpha}_{tt}\Delta T\right)\,\mathrm{d}b \;=\; Ah\left(\xi_{tt}^i + ek_n^i - \hat{\alpha}_{tt}^i\Delta T\right)\\
F_n^i &= \int_h Q_t^i \,\mathrm{d}b \;=\; A_{55}^{\mathrm{s}} h 2\xi_{tn}^i\\
F_b^i &= \int_h N_{tb}^i \,\mathrm{d}b \;=\; Fh\left(2\xi_{tb}^i - \hat{\alpha}_{tb}^i\Delta T\right)\\
M_t^i &= \alpha\int_h M_{tb}^i \,\mathrm{d}b \;=\; \alpha Hhk_t^i \quad \text{with } \alpha = 4 \quad \text{(see Ref. [44])}\\
M_n^i &= \int_h N_{tt}^i b \,\mathrm{d}b \;=\; Ah\left[e\xi_{tt}^i + \left(\frac{h^2}{12} + e^2\right)k_n^i - e\hat{\alpha}_{tt}^i\Delta T\right]\\
M_b^i &= \int_h M_{tt}^i \,\mathrm{d}b \;=\; Dbk_b^i
\end{aligned}
\tag{70}
$$

where $e = \frac{1}{2}\left(t + h\right)$ is the stiffener eccentricity.

$$
\begin{Bmatrix} F_t^i \\ F_n^i \\ F_b^i \\ M_t^i \\ M_n^i \\ M_b^i \end{Bmatrix} = \begin{bmatrix} Ah & 0 & 0 & 0 & Ahe & 0 \\ 0 & A_{55}^{\mathrm{s}}h & 0 & 0 & 0 & 0 \\ 0 & 0 & Fh & 0 & 0 & 0 \\ 0 & 0 & 0 & 4Hh & 0 & 0 \\ Ahe & 0 & 0 & 0 & Ah\left(\frac{h^2}{12} + e^2\right) & 0 \\ 0 & 0 & 0 & 0 & 0 & Dh \end{bmatrix} \begin{Bmatrix} \xi_{tt}^i \\ 2\xi_{tn}^i \\ 2\xi_{tb}^i \\ k_t^i \\ k_n^i \\ k_b^i \end{Bmatrix} - \begin{Bmatrix} Ah\hat{\alpha}_{tt}^i \\ 0 \\ Fh\hat{\alpha}_{tb}^i \\ 0 \\ Ahe\hat{\alpha}_{tt}^i \\ 0 \end{Bmatrix} \Delta T \tag{71}
$$

or, in compact form:

$$
\begin{Bmatrix} \mathbf{F}^i \\ \mathbf{M}^i \end{Bmatrix} = \mathbf{C}^i \begin{Bmatrix} \boldsymbol{\xi}^i \\ \mathbf{k}^i \end{Bmatrix} - \begin{Bmatrix} \hat{\mathbf{F}}^i \\ \hat{\mathbf{M}}^i \end{Bmatrix} \Delta T \tag{72}
$$

where the beam section constitutive law $\mathbf{C}^i$ and the vectors of unitary thermal loads $\hat{\mathbf{F}}^i$ and $\hat{\mathbf{M}}^i$ are available by comparison between Eq. (72) and Eq. (71).

5.3. Ply angles

Example 1

$$\text{Design 1:}\quad \theta_1 = \begin{bmatrix} 68 & 55 & 19 \end{bmatrix} \qquad \theta_2 = \begin{bmatrix} -76 & -55 & 9 \end{bmatrix} \tag{73}$$

$$\text{Design 2:}\quad \theta_1 = \begin{bmatrix} 71 & 49.5 & 71.5 \\ 67 & 50 & 51 \\ 17 & 12 & 45 \end{bmatrix} \qquad \theta_2 = \begin{bmatrix} -72.5 & -59 & -59.5 \\ -65 & -54 & -50.5 \\ 14 & 11.5 & 6 \end{bmatrix} \tag{74}$$

$$\text{Design 3:}\quad \theta_1 = \begin{bmatrix} 71 & 49.5 & 71.5 \\ 67 & 50 & 51 \\ 17 & 12 & 45 \end{bmatrix} \qquad \theta_2 = -\begin{bmatrix} 89 & 67.5 & 64 & 65 & 82 \\ 81 & 69 & 65 & 60 & 60 \\ 80.5 & 66.5 & 58 & 54.5 & 59 \\ 26 & 25 & 18 & 24 & 25 \\ 8 & -4.5 & 1 & -5 & -0 \end{bmatrix} \tag{75}$$

Pre-stressed vibrations

$\Delta\overline{u}/\Delta\overline{u}^{\mathrm{qi}} = 0.0$

$$\theta^{\mathrm{SSSS}} = \begin{bmatrix} 48.36 & 47.40 & 43.38 \\ 43.60 & 44.65 & 46.29 \\ 55.22 & 46.06 & 44.25 \end{bmatrix} \quad \theta^{\mathrm{SCSC}} = \begin{bmatrix} 90 & 90 & 65.37 \\ 90 & 60.55 & 37.70 \\ 90 & 90 & 65.04 \end{bmatrix} \quad \theta^{\mathrm{CCCC}} = \begin{bmatrix} 86.41 & 56.45 & -16.72 \\ 64.35 & 45.62 & -0.15 \\ 90 & 90 & 15.88 \end{bmatrix} \tag{76}$$

$\Delta\overline{u}/\Delta\overline{u}^{\mathrm{qi}} = 0.1$

$$\theta^{\mathrm{SSSS}}_{=} \begin{bmatrix} 90.00 & 89.67 & 46.35 \\ 90.00 & 53.95 & 48.68 \\ 90.00 & 45.86 & 51.69 \end{bmatrix} \quad \theta^{\mathrm{SCSC}} = \begin{bmatrix} 90.00 & 90.00 & 76.01 \\ 90.00 & 65.39 & 34.61 \\ 90.00 & 90.00 & 70.38 \end{bmatrix} \quad \theta^{\mathrm{CCCC}} = \begin{bmatrix} 90.00 & 66.36 & -17.35 \\ 90.00 & 50.20 & 44.65 \\ 90.00 & 90.00 & 46.78 \end{bmatrix} \tag{77}$$

$\Delta\overline{u}/\Delta\overline{u}^{\mathrm{qi}} = 0.5$

$$\theta^{\mathrm{SSSS}} = \begin{bmatrix} 90.00 & 90.00 & 86.87 \\ 90.00 & 72.52 & 39.80 \\ 90.00 & 56.13 & 44.37 \end{bmatrix} \quad \theta^{\mathrm{SCSC}} = \begin{bmatrix} 90.00 & 90.00 & 90.00 \\ 90.00 & 77.55 & 31.00 \\ 88.72 & 90.00 & 78.54 \end{bmatrix} \quad \theta^{\mathrm{CCCC}} = \begin{bmatrix} 90.00 & 76.62 & -16.92 \\ 89.92 & 68.58 & -9.05 \\ 87.93 & 90.00 & 65.20 \end{bmatrix} \tag{78}$$

$\Delta\overline{u}/\Delta\overline{u}^{\mathrm{qi}} = 1.0$

$$\theta^{\mathrm{SSSS}} = \begin{bmatrix} 87.98 & 89.78 & 90.00 \\ 87.06 & 90.00 & 39.36 \\ 90.00 & 69.16 & 31.70 \end{bmatrix} \quad \theta^{\mathrm{SCSC}} = \begin{bmatrix} 89.30 & 90.00 & 76.01 \\ 89.69 & 82.50 & 35.34 \\ 87.71 & 90.00 & 77.80 \end{bmatrix} \quad \theta^{\mathrm{CCCC}} = \begin{bmatrix} 83.66 & 80.32 & -19.24 \\ 86.53 & 78.94 & -36.19 \\ 89.50 & 90.00 & 90.00 \end{bmatrix} \tag{79}$$

Example 3

Buckling analysis and pre-stressed vibrations

$$\theta_1 = \begin{bmatrix} 71 & 49.5 & 71.5 \\ 67 & 50 & 51 \\ 17 & 12 & 45 \end{bmatrix} \qquad \theta_2 = \begin{bmatrix} -72.5 & -59 & -59.5 \\ -65 & -54 & -50.5 \\ 14 & 11.5 & 6 \end{bmatrix} \tag{80}$$

5.4. Control points

Table 10: Position of control points – Example 3.

	Stiffener 1		Stiffener 2		Stiffener 3		Stiffener 4	
Point	x	y	x	y	x	y	x	y
1	-150.00	-112.50	-112.50	150.00	150.00	112.50	112.50	-150.00
2	-17.16	-73.04	14.84	92.64	13.73	77.44	-27.46	-111.68
3	109.56	10.12	100.11	-23.00	-91.17	-24.71	-143.48	-1.00
4	150.00	150.00	150.00	-150.00	-150.00	-150.00	-150.00	150.00

Table 11: Position of control points – Example 4.

	Stiffener 1		Stiffener 2	
Point	x	y	x	y
1	-75.00	0	-37.50	-75.00
2	-29.24	16.80	-6.00	-34.70
3	11.24	42.93	37.92	-17.80
4	37.50	75.00	75.00	0